



# Seasonal variation of atmospheric pollutants transport in central Chile: dynamics and consequences

Rémy Lapere<sup>1</sup>, Laurent Menut<sup>1</sup>, Sylvain Mailler<sup>1,2</sup>, and Nicolás Huneeus<sup>3</sup>

<sup>1</sup>Laboratoire de Météorologie Dynamique, IPSL, École Polytechnique, Institut Polytechnique de Paris, ENS, Université PSL, Sorbonne Université, CNRS, Palaiseau, France

<sup>2</sup>École des Ponts, Université Paris-Est, 77455 Champs-sur-Marne, France

<sup>3</sup>Department of Geophysics, Universidad de Chile, Santiago, Chile

**Correspondence:** Rémy Lapere (remy.lapere@lmd.ipsl.fr)

**Abstract.** Central Chile faces atmospheric pollution issues all year long, in relation with elevated concentrations of fine particulate matter during the cold months and tropospheric ozone during the warm season. In addition to public health issues, environmental problems regarding vegetation growth and water supply, as well as meteorological feedback are at stake. Sharp spatial gradients in regional emissions along with a complex geographical situation make for variable and heterogeneous dynamics in the localization and long-range transport of pollutants, with seasonal differences. Based on chemistry-transport modeling with WRF-CHIMERE, this work studies for one winter period and one summer period: (i) the contribution of emissions from the Santiago Metropolitan Area to air pollution in central Chile, (ii) the reciprocal contribution of regional pollutants transported into the Santiago basin. The underlying 3-dimensional advection patterns are investigated. We find that on average for the winter period  $5 \mu\text{g m}^{-3}$  to  $10 \mu\text{g m}^{-3}$  of fine particulate matter in Santiago come from regional transport, corresponding to 13% to 15% of average concentrations. In turn, emissions from the Metropolitan Area contribute to 5% to 10% of fine particulate matter pollution as far as  $4^\circ$  north and  $4^\circ$  south. Wintertime transport occurs mostly close to the surface. In summertime, exported precursors from Santiago, in combination with mountain-valley circulation dynamics, are found to account for most of ozone formation in the adjacent Andes cordillera and to create a persistent plume of ozone of more than 50 ppb, extending along 80 km horizontally and 1.5 km vertically, and located several hundred meters above ground, slightly north of Santiago. This work constitutes the first description of such an ozone bubble formation mechanism. Emissions of precursors from the capital city also affect daily maxima of surface ozone hundreds of kilometers away. In parallel, cutting emissions of precursors in the Santiago basin results in an increase of surface ozone mixing ratios in its western area.

## 1 Introduction

Most urban areas in central Chile, including the capital city Santiago, deal with harmful atmospheric concentrations of fine particulate matter ( $\text{PM}_{2.5}$ ) in wintertime (Saide et al., 2016; Barraza et al., 2017; Toro et al., 2019; Lapere et al., 2020), and tropospheric ozone ( $\text{O}_3$ ) in summertime (Gramsch et al., 2006; Seguel et al., 2013, 2020). Strong anthropogenic emissions of primary pollutants and precursors, combined with the poor ventilation conditions induced by the topography and synoptic-scale circulation, are the core reasons for such air quality issues (Rutllant and Garreaud, 1995). The main sources of atmospheric



pollutants in Santiago are road traffic and industrial activities, with additional contributions in wintertime from wood burning  
25 for residential heating (Barraza et al., 2017; Mazzeo et al., 2018). Such characteristics apply to most urban areas in central  
Chile, including coastal zones (Sanhueza et al., 2012; Toro et al., 2014; Marín et al., 2017).

This region is home to more than 12 million people, who are chronically exposed to PM<sub>2.5</sub> pollution, leading to respiratory  
and cardiovascular issues (Ilabaca et al., 1999; Soza et al., 2019). Chronic and acute exposures to PM<sub>2.5</sub> pollution also induce  
a significant economic burden (MMA, 2012; OECD, 2016). A side effect is the deposition of light-absorbing particulate matter  
30 on the adjacent Andean snowpacks (Rowe et al., 2019; Lapere et al., 2021) contributing to the observed accelerated melting  
of glaciers. Aerosols also affect the radiative balance of the atmosphere and influence cloud formation by acting as cloud  
condensation nuclei (e.g. Chung and Seinfeld, 2005; Koch and Genio, 2010). Tropospheric O<sub>3</sub> is a secondary pollutant formed  
by the photochemical oxidation of volatile organic compounds (VOC) in the presence of nitrogen oxides (NO<sub>x</sub>). The essential  
role of photolysis in its production explains that harmful levels are mostly observed in summertime (e.g. Walcek and Yuan,  
35 1995; Seinfeld and Pandis, 2006). O<sub>3</sub> is noxious for human health, causing respiratory disorders such as asthma (Lippmann,  
1991). Furthermore, its deposition on plant leaves affects their photosynthesis and evaporation ability, hence damaging crop  
yields (Hill and Littlefield, 1969). Tropospheric O<sub>3</sub> is also a powerful greenhouse gas (GHG) as well as a photochemical  
oxidant hence playing a key role in the atmosphere.

Although anthropogenic urban pollution is mostly a phenomenon affected by local sources and meteorology, interactions  
40 with remote emissions and air masses also occur. Depending on the wind system and stability of the troposphere, pollutants and  
precursors can be transported far from the emission site and reach distant locations. Urbanized areas in Europe (Vardoulakis  
and Kassomenos, 2008) and South America (Resquin et al., 2018) usually feature a marked contribution of long-range transport  
to measured concentrations of particulate matter within urban basins. For Santiago, an example can be found in the wildfires  
occurring frequently in summertime in central Chile, explaining sporadic peaks of particulate matter and ozone in the city  
45 although the sources are found more in the South (Rubio et al., 2015; de la Barrera et al., 2018). In this case, pollutants are not  
directly of anthropogenic origin, which is out of the scope of the present work and hence not considered. Generally speaking,  
the processes and patterns underlying anthropogenic pollutants transport at the scale of central Chile are not well known, nor  
is the amount of advected contaminants.

Chile is a narrow band of land bordered by the Pacific ocean on the western side and the Andes cordillera on the eastern  
50 side. Air motions are thus influenced by sea-land atmospheric interactions and mountain-valley circulation, in addition to more  
synoptic patterns. The intensity of these atmospheric regimes, which are partly governed by radiative processes, are modulated  
seasonally. So do emissions of primary pollutants and photochemical reactions involved in the creation of secondary pollutants  
(e.g. Gramsch et al., 2006; Barraza et al., 2017). Moreover, despite a well developed network of air quality monitoring stations  
across the country, the spatial and temporal density of the data does not allow for a detailed observation-based study of  
55 atmospheric pollutants transport. As a result, chemistry-transport modeling offers a solution to cope with this issue and provide  
insights regarding the magnitude and mechanisms of advection of pollutants at the regional scale.

The present work studies, for one summer month and one winter month in 2015 in central Chile, through chemistry-  
transport simulations with WRF-CHIMERE, (i) the contribution of pollutants emitted in Santiago to the regional atmospheric



composition, (ii) the reciprocal contribution of regional emissions to air pollution in the capital city basin, (iii) the corresponding  
60 3-dimensional advection patterns of particulate matter and ozone. The methodology and data are described in Section 2, the  
relative contributions of transport and the underlying advection processes are presented in Section 3. These results are discussed  
in Section 4 and conclusions are gathered in Section 5.

## 2 Data and methods

### 2.1 Modeling setup

65 The chemistry-transport simulations are performed with the Weather Research and Forecasting (WRF) mesoscale numerical  
weather model from the US National Center for Atmospheric Research (Skamarock et al., 2008) to simulate the meteorological  
fields, and CHIMERE to compute chemistry and transport (Mailler et al., 2017). Anthropogenic emissions are based on the  
EDGAR HTAP V2 inventory (Janssens-Maenhout et al., 2015). The simulation domain has a 5 km spatial resolution, extending  
over 200 latitudinal and 100 longitudinal grid points, and is centered on Santiago (white domain CHILE\_5K in Figure 1a). The  
70 parameterizations and model configuration used for WRF are presented in Table A1. WRF is applied to 60 vertical levels up  
to the highest elevation of 50 hPa. Initial and boundary conditions rely on the NCEP FNL analysis data sets, with a 1° by 1°  
spatial resolution and 6-hour temporal resolution, from the Global Forecast System (NCEP, 2000). Land-use and orography  
are extracted from the modified IGBP MODIS 20-category database with 30 sec resolution (Friedl et al., 2010). CHIMERE  
is a Eulerian 3-dimensional regional Chemistry-Transport Model, able to reproduce gas-phase chemistry, aerosols formation,  
75 transport and deposition. In this work, the 2017 off-line version of CHIMERE is used (Mailler et al., 2017). The model  
configuration is described in Table A1, with the same horizontal domain as for WRF, applied on 30 vertical levels up to 150 hPa.  
Emissions from the EDGAR HTAP V2 inventory are downscaled and split in time down to daily/hourly rates following the  
methodology of Menut et al. (2013).

Two different simulation periods are investigated to account for summertime and wintertime differences in atmospheric  
80 composition and advection dynamics. "Summertime" hereafter refers to the simulated period 4 January to 3 February 2015. A  
20-days spin-up period between 15 December 2014 and 3 January 2015 is used. "Wintertime" refers to the simulated period  
between 1 July and 31 July 2015. A spin-up period from 15 June to 30 June 2015 is applied. For each of these periods,  
two simulations are performed. One uses a full emissions inventory including all emissions within the region, referred to as  
"baseline" henceforth. The baseline simulation for wintertime is named "WB" and the baseline simulation for summertime  
85 is denoted "SB". The second simulation corresponds to the case where the area of Santiago would emit no anthropogenic  
pollutants. In this regard, all anthropogenic emissions within the area corresponding to the white rectangle in Figures 1b  
through 1e are set to zero in the simulation referred to as "contribution", hence the designation "WC" and "SC" for the  
corresponding wintertime and summertime simulations, respectively. The difference in simulated concentrations between  
baseline and contribution runs shows the proportion of pollutants transported to and exported from Santiago. Aerosol feedback  
90 on meteorology is not taken into account here in order to isolate the sensitivity to emission rates only, so that for a given  
season the same WRF fields are used for both emission cases. Emissions downscaled from the HTAP V2 inventory and input

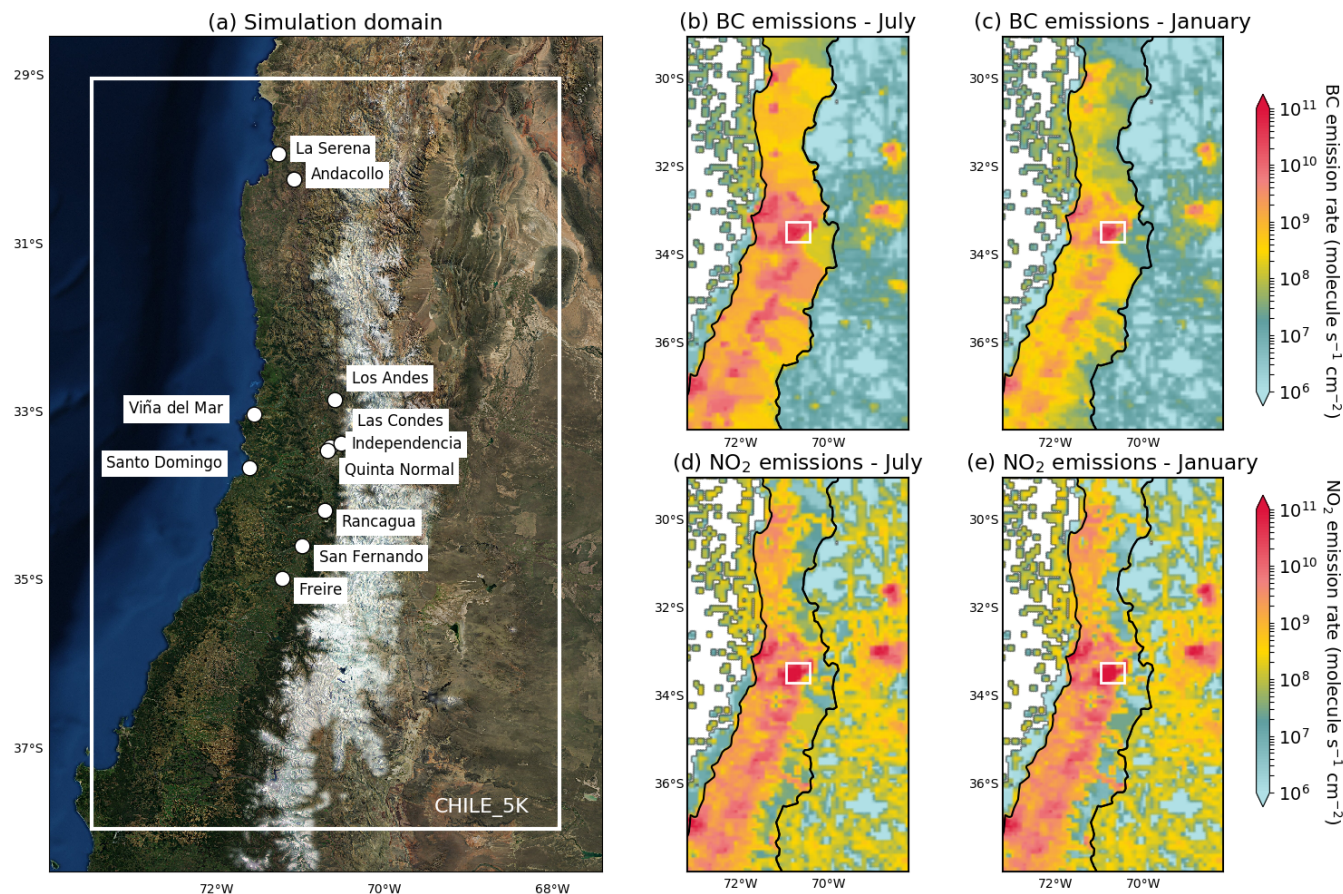


**Figure 1.** (a) Simulation domain at 5 km spatial resolution centered over Santiago. Locations of interest are designated with white dots. Map background layer: Imagery World 2D, ©2009 ESRI. (b) Daily average surface emission rate of BC for July 2015, (c) same as (b) for January 2015, (d) same as (b) for NO<sub>2</sub>, (e) same as (d) for January 2015.

into CHIMERE are shown in Figures 1b through 1e. The seasonality of BC emissions is clear, given the major role played by residential heating which takes place mostly in wintertime. Monthly NO<sub>2</sub> emissions are less variable throughout the year, related to the sustained traffic and industrial sources that are nearly constant through time. Figures 1b through 1e also evidence that the region of Santiago (represented with a white rectangle) features the highest emission rates for both pollutants and dominates the signal over the simulation domain. In the continuation, given their relevance for the associated seasons, PM<sub>2.5</sub> in wintertime and O<sub>3</sub> and its precursors in summertime will be considered as the variables of interest, although PM<sub>2.5</sub> in summertime and O<sub>3</sub> in wintertime can be occasionally discussed.



## 2.2 Simulation validation

100 Surface meteorology and pollutants concentrations are validated using data from the automated air quality and meteorology monitoring network of Chile, known as Sistema de Información Nacional de Calidad del Aire (<https://sinca.mma.gob.cl/index.php/>, last access October 1 2020). Different stations across central Chile are considered depending on data availability for the simulated periods (stations locations can be found in Figure 1a). Meteorological vertical profiles in downtown Santiago, for a few days in July 2015, were provided by the Chilean meteorological office, Dirección Meteorológica de Chile.

105 Simulation scores for surface and vertical profile meteorology are gathered in Tables A2 and A3. Biases on daily mean temperature range between  $-1.23^{\circ}\text{C}$  and  $0.31^{\circ}\text{C}$  in wintertime except for the mountainous location of Los Andes where the bias reaches  $-3.33^{\circ}\text{C}$ . In summertime the bias is between  $0.07^{\circ}\text{C}$  to  $0.67^{\circ}\text{C}$ . For both periods, correlations on surface temperature vary between 0.7 and 0.89, except for Viña del Mar where it drops to 0.25 in wintertime and 0.18 in summertime, which can be explained by the location of this station near the ocean. The corresponding grid point in the model straddles ocean  
110 and land hence featuring a strong gradient, and as a result may not be representative of this coastal city. This remark applies to all meteorological variables at coastal sites. The model is a little too dry with average biases on surface relative humidity of  $-15\%$  to  $-20\%$  but shows fair correlations around 0.8 to 0.9. Surface winds are fairly reproduced, with limited biases and wind gusts well captured, although the correlations can be low for some locations. Figures A1 and A2 compare observed and simulated surface wind distributions for four sites. Summertime shows a good reproduction of wind regimes for all locations,  
115 expect for a small positive bias on speeds. In wintertime, winds are more variable and follow less clear patterns, so that the model performance is not as good, especially for the coastal locations of La Serena and Santo Domingo. A positive bias on speed is also observed. Most features of the vertical profiles of temperature, relative humidity and winds are well reproduced, with very good correlations and limited biases for four winter days in downtown Santiago (Tab. A3). On the whole, these statistics give confidence in the ability of the model to produce realistic transport events for both seasons.

120 Figure 2 shows a scatter plot of measured and modeled daily mean concentrations of  $\text{PM}_{2.5}$  in wintertime and daily maximum mixing ratio of  $\text{O}_3$  in summertime. For  $\text{PM}_{2.5}$  the simulation performs better for sites far inland with correlations of 0.77 and 0.69 for Rancagua and Independencia, respectively. Correlations for the two coastal sites considered (Viña del Mar and La Serena) are more moderate with 0.34 and 0.25, respectively. The same issue of straddling grid points explained previously leads to these degraded statistics: while observations at these sites show a chaotic time series, the model produces a smoother diurnal  
125 cycle due to the grid point being partially over the ocean. However for those two sites, biases remain small, while the model systematically underestimates concentrations in Rancagua, and slightly overestimates  $\text{PM}_{2.5}$  in Santiago (Independencia). For  $\text{O}_3$  the picture is similar with a good reproduction of daily peaks in summertime. Despite the relatively coarse resolution of the simulation and strong spatial heterogeneity in precursors emissions, limited biases of a few ppb are obtained on  $\text{O}_3$  peaks in summertime, down to only 1 ppb at the most  $\text{O}_3$ -polluted site of Las Condes (northeastern Santiago). The diurnal cycle of  $\text{O}_3$   
130 is also well reproduced with hourly correlations (not shown here) of 0.67 for Viña del Mar and 0.8 to 0.9 for the three other sites. In parallel, summertime  $\text{NO}_x$  mixing ratios within the Santiago area (not shown here) are well captured by the model

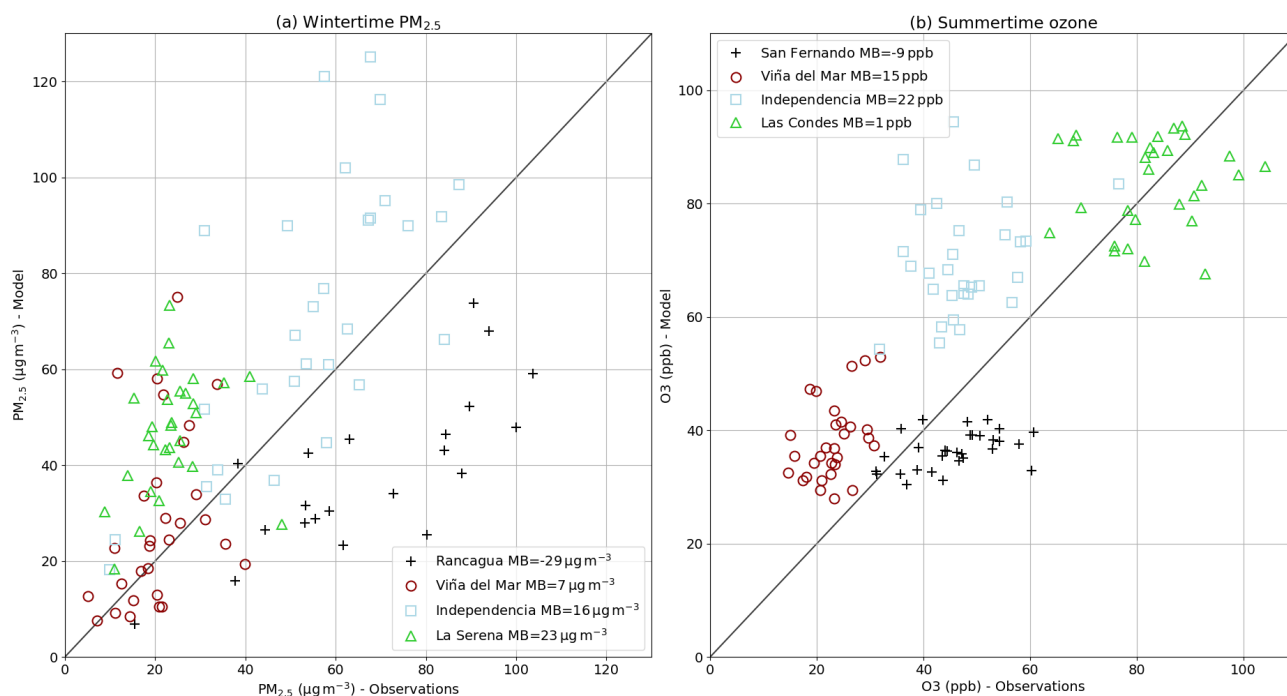


**Figure 2.** Comparison between observation and simulation for (a) wintertime daily average PM<sub>2.5</sub> concentrations, (b) summertime daily maximum O<sub>3</sub> mixing ratio. Wintertime and summertime correspond to the periods defined in Section 2.1, respectively. MB is the mean bias.

with mean biases between 0.05 and 1.23 ppb for three stations in Santiago (Las Condes, Puente Alto - southeastern Santiago - and Independencia), associated with decent hourly correlations between 0.43 and 0.59.

The lack of available data for NO<sub>x</sub> at other locations in central Chile, and more generally VOC data for all locations makes the simulation validation impossible for these precursors. However, the good reproduction of both O<sub>3</sub> and NO<sub>x</sub> advocates in favor of the production of adequate levels of VOC, at least in the Santiago area. In addition, although such a work is yet to be done for Chile, comparisons of HTAP emissions of VOC with more refined national inventories in South America show that despite a spatial distribution and speciation profile with margin for improvement, total amounts of emitted VOC as provided by HTAP are well in the range of higher resolution inventories based on local observations for Argentina (Puliafito et al., 2017) and São Paulo (Dominutti et al., 2020). In parallel, emissions of NO<sub>x</sub> and PM<sub>10</sub> from HTAP for the region of Santiago show similar biases and discrepancies as other mega-cities in South America such as Buenos Aires and Rio de Janeiro (Huneus et al., 2020), so that we can assume this similarity also applies for VOC. By extension, if HTAP for Santiago is comparable to HTAP for Argentinian and Brazilian mega-cities, where VOC total emitted amounts are adequately provided by HTAP, VOC emissions for Santiago likely have the appropriate magnitude as well, despite some discrepancies. Besides, the aforementioned discrepancies are critical when it comes to more detailed approaches for policy making but for the purpose of the present work, having the proper total amount is sufficient as we apply our own downscaling methodology, do not discuss very high-resolution processes, and rely mostly on sensitivity analysis.



In conclusion,  $PM_{2.5}$  in wintertime and  $O_3$  and its precursors in summertime, the key pollutants for their respective seasons, as well as meteorological conditions, are fairly reproduced by the model for a selection of sites throughout central Chile, which gives confidence in the model outputs that are described and analyzed in the following sections.

### 3 Results

The semi-permanent South Pacific High, centered around ( $30^\circ S$ ,  $110^\circ W$ ), along with the elevated Andes cordillera, are two large-scale drivers of the surface wind systems in central Chile. The persistent high induces high velocity southwesterlies blowing along the coast during both daytime and nighttime (Fig. 3). These also penetrate deep into land as far as the Andes in summertime during the day, before being blocked by the mountains. On the other side of the cordillera, less intensive easterlies coming from Argentina encounter the foothills. Also, the presence of the Andes leads to the development of mountain-valley circulation patterns (e.g. Whiteman, 2000) when the differential heating between narrow valleys and wide plains at the onset and offset of the day lead to the creation of upslope westerlies during daytime (as seen in Fig. 3b), and a reversal at nighttime with downslope easterlies (Fig. 3d). Although this pattern can be perturbed by clouds or synoptic-scale transient phenomena such as coastal lows, it represents the typical surface wind diurnal cycle for basins along the cordillera. From these mean wind fields, the dominant advection pathways of pollutants can be inferred. Polluted air masses are on average blown towards the cordillera and the north during daytime in summertime, and have more complex dynamics in wintertime but also transport northward in general. Deeper and more turbulent planetary boundary layer heights during daytime, as observed in summertime (Fig. 3a) also enable the vertical export of pollutants up into the free troposphere (FT) where they can be advected farther, while wintertime shallower boundary layers (Fig. 3b) imply more stagnation of air masses.

#### 3.1 Impact of emissions from Santiago on regional atmospheric composition

##### 3.1.1 Wintertime $PM_{2.5}$

Consistently with the mean wind fields and emission rates of pollutants in central Chile discussed previously, anthropogenic emissions in the Metropolitan Area of Santiago significantly influence surface atmospheric composition over a large region, over land, the Andes and the Pacific ocean. The following results are based on the analysis of sensitivity to emissions from Santiago described in Section 2.1: the difference between the simulation with (baseline case) and without (contribution case) emissions from Santiago yields their contribution to atmospheric composition over the domain. Figures 4a and 4b show the average wintertime  $PM_{2.5}$  plume (absolute and relative, respectively) attributable to emissions from the capital area. The direct western vicinity of the Santiago basin receives, on average  $5 \mu g m^{-3}$  to  $15 \mu g m^{-3}$  coming from the capital, a few tens of kilometers from the source, corresponding to more than 30% of the signal simulated in the baseline scenario for this area. At the scale of hundreds of kilometers, the export drops to a few  $\mu g m^{-3}$ , corresponding to 5% to 20%. It is worth noting that the relative contribution of emissions from Santiago remains greater than 5% on a area as large as more than  $8^\circ$  meridionally and  $3^\circ$  zonally, hence stressing the significant impact of the capital on atmospheric composition for the whole region (Fig. 4b).

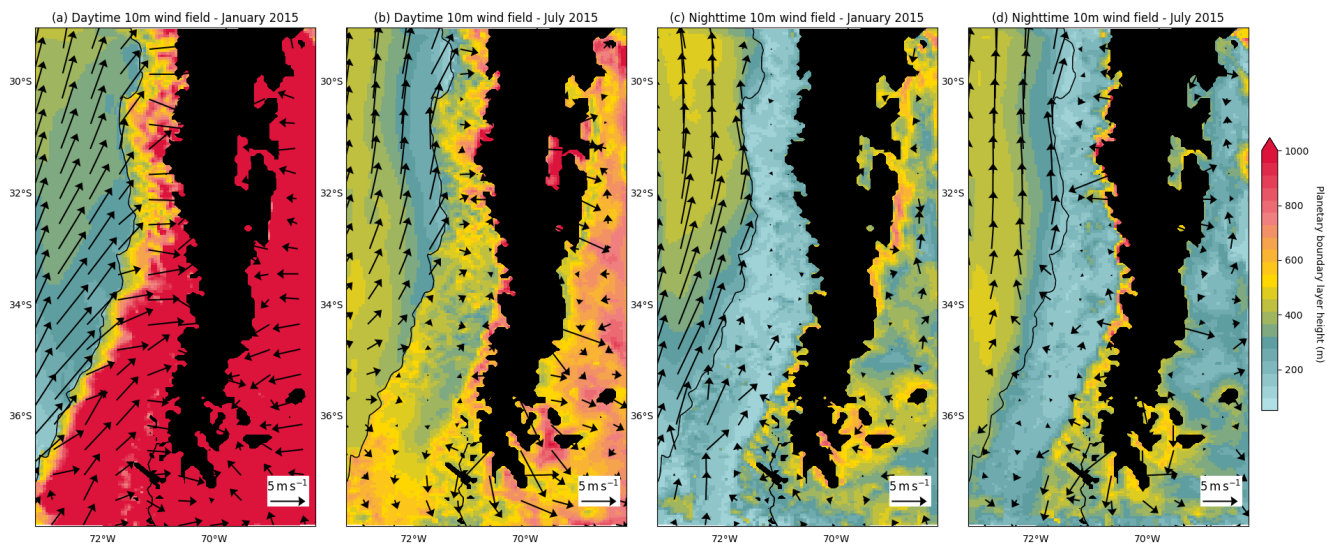


**Figure 3.** Average 10 m wind field (arrows) and planetary boundary layer height (colormap) simulated by WRF (a) during daytime in January 2015, (b) during daytime in July 2015, (c) during nighttime in January 2015, (d) during nighttime in July 2015. Black areas show grid points with elevation in excess of 2000 m a.s.l.

In particular, the southern part of the plume is transported over the Andes down to Argentina with a large spread of several  
180 degrees of longitude, whereas the northern part extends mostly along the coast in a narrower manner and transports as far as  
the boundary of the simulation domain.

More specifically, urban areas along the north-south axis of Santiago (Curicó, San Fernando, Rancagua and Los Andes in  
Fig. 4a) receive  $1 \mu\text{g m}^{-3}$  to  $2 \mu\text{g m}^{-3}$  from Santiago on a hourly basis on average, corresponding to 4% to 8% of the baseline  
concentrations (Fig. 4c). Sporadically, up to more than  $20 \mu\text{g m}^{-3}$  in Rancagua and  $9 \mu\text{g m}^{-3}$  in San Fernando, Curicó and Los  
185 Andes can be attributed to emissions from Santiago. These significant contributions likely lead to alert thresholds crossing for  
some hours in these cities.

On the eastern side of the Santiago basin is the Andes cordillera. We examine the contribution of Santiago emissions in a  
village (San Gabriel) and a summit (Maipo volcano) along the Maipo canyon, southeast of Santiago. We find that for the village  
 $34\%$  ( $1 \mu\text{g m}^{-3}$ ) of  $\text{PM}_{2.5}$ , on average, is transported from the metropolitan area. This is consistent with the mountain-valley  
190 circulation patterns aforementioned, leading to the intrusion of urban air masses deep into the canyon (Lapere et al., 2021). We  
acknowledge that the estimate of 34% is probably larger than reality since the HTAP inventory does not capture properly local  
emissions in the village of San Gabriel, which likely dominate the signal, especially with wood burning for residential heating  
being largely used in such villages in wintertime. In the Maipo volcano area (summit at 5264 m a.s.l.), a small contribution in  
absolute value is found (less than  $0.5 \mu\text{g m}^{-3}$ ) although it can reach up to more than  $2 \mu\text{g m}^{-3}$  occasionally, but this corresponds  
195 to 20% of the signal there on average. This area is covered in snow during wintertime, so that despite the small magnitude of





the import of  $PM_{2.5}$  it can lead to significant radiative effects when deposited, especially given the large fraction of black carbon in  $PM_{2.5}$  emitted in Santiago (around 15% at Independencia - not shown here).

The Viña del Mar-Valparaíso area is the second largest populated region of Chile, located on the ocean coast west of Santiago. In wintertime, it is downwind of Santiago, which leads to an average import of particulate matter from the capital city of  $3 \mu g m^{-3}$  (18%) and sporadically up to  $18 \mu g m^{-3}$ . Again, air quality in this urban area is worsened by export from Santiago, by a significant share. Further north, at the location of La Serena, which also suffers from bad air quality in wintertime, the contribution of Santiago emissions is more moderate but still remains significant in absolute value although its contribution is only 1%.

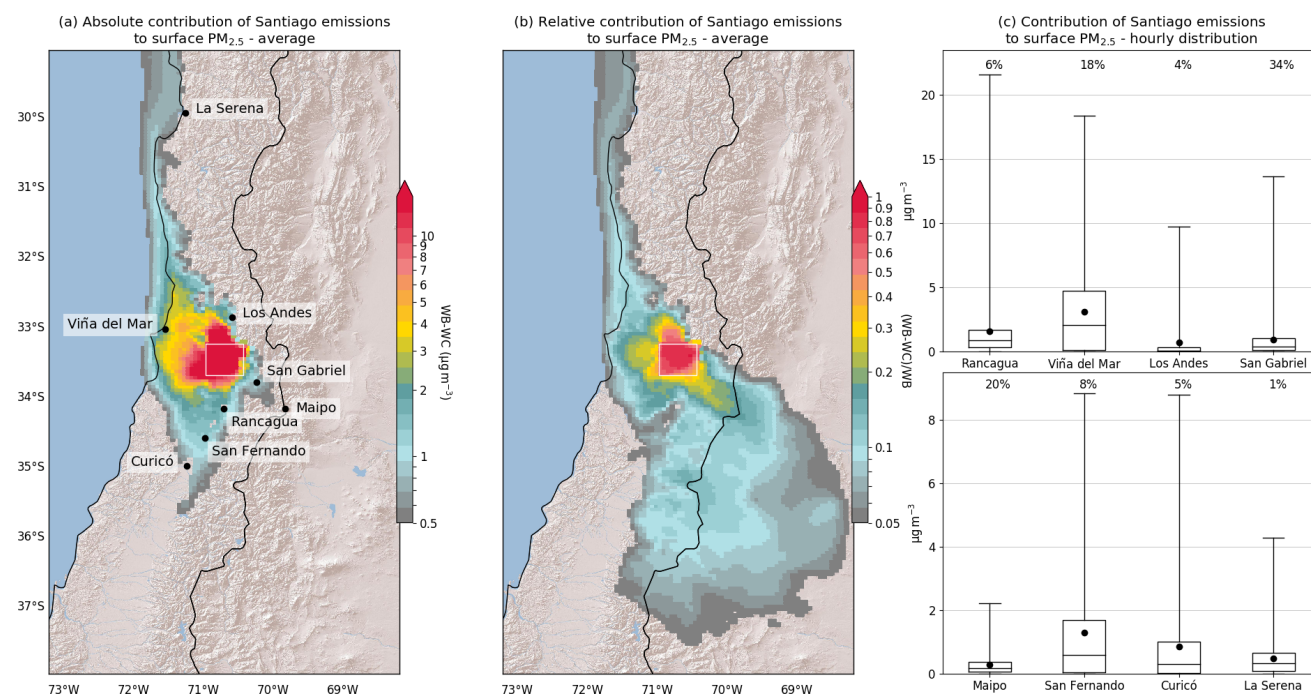


**Figure 4.** (a) Average ground-level  $PM_{2.5}$  concentration difference between WB (winter baseline case) and WC (winter contribution case) yielding the Santiago emissions contribution. Concentrations in excess of  $0.5 \mu g m^{-3}$  are displayed. White rectangle shows the area where emissions are set to zero in WC. Map background layer: World Shaded Relief, ©2009 ESRI, (b) same as (a) in relative contribution i.e.  $(WB-WC)/WB$ . Contributions in excess of 5% are displayed. (c) Distribution of Santiago emissions contribution to hourly  $PM_{2.5}$  concentration at several sites across central Chile - horizontal lines are quartiles, whiskers show minimum and maximum, dots are the means. All figures are based on hourly concentrations and are for wintertime 2015. In panels (a) and (b) only grid points where the distribution of concentrations in scenario WC is different than in scenario WB at the 90% level, based on a t-test, are shown.



### 3.1.2 Summertime O<sub>3</sub>

205 In summertime, except for PM<sub>2.5</sub> emitted by biomass burning events (not considered here), O<sub>3</sub> is the pollutant raising concern. Combined significant emissions of NO<sub>x</sub> and VOC are required, in the presence of sunlight, to generate high mixing ratios of O<sub>3</sub>. However, a lot of non-linearities are involved in the tropospheric O<sub>3</sub> cycle, so that the sensitivity to its precursors emissions is not straightforward. For instance, imbalances in the ratio of NO<sub>x</sub> and VOC decrease O<sub>3</sub> formation. Given the crucial role of photolysis in O<sub>3</sub> formation, it features a strong diurnal cycle, with levels coming back to low values at night. Thus, the  
210 important variable to determine whether O<sub>3</sub> pollution is high is its daily maximum mixing ratio, on which we will mostly focus hereafter.

Figure 5a shows the average of maximum hourly O<sub>3</sub> mixing ratio at ground-level observed each day in the baseline case (SB). In the baseline scenario, O<sub>3</sub> is mostly found at harmful levels near the area of Santiago, and mainly on its eastern side. Again, mountain-valley circulation accounts for this observation: afternoon westerlies blow O<sub>3</sub> precursors, present in large  
215 amounts in urban air masses, towards the Andes. NO<sub>x</sub> lifetime is a few hours at most, depending on the reactivity of VOC and NO<sub>2</sub> density (e.g. Laughner and Cohen, 2019), while most VOC have an atmospheric lifetime of several days (e.g. Monod et al., 2001), so that on the way, NO<sub>x</sub> are more consumed than VOC. Consequently, while urban air is mostly a NO<sub>x</sub>-rich environment, precursors ratios become more balanced along with the export so as to create more favorable conditions for O<sub>3</sub> formation once reaching less urbanized areas. Such a mechanism is observed for Paris and its suburbs for instance (e.g. Menut  
220 et al., 2000). Export by easterlies occur less frequently and mostly at night when O<sub>3</sub> cannot be created due to lack of sunlight, which is why the rural area west of Santiago shows smaller O<sub>3</sub> maxima. This mechanism explains the large concentrations of O<sub>3</sub> mostly found east of Santiago. Except for the center part of the domain where average daily maxima reach more than 100 ppb, O<sub>3</sub> pollution is less concerning elsewhere in central Chile where they range between 10 ppb and 35 ppb.

Figure 5b shows the decrease in O<sub>3</sub> daily maxima induced by eliminating emissions of the Santiago basin. The spatial pattern  
225 is again consistent with the mechanism introduced previously: emissions of precursors from Santiago are the main origin for O<sub>3</sub> formation in the cordillera and north of the city, with a reduction of more than 50 ppb of the daily maxima over this area when the capital city no longer emits pollutants.

More specifically, the northern city of Los Andes shows a decrease of its daily maxima by 15 ppb on average (Fig. 5b) while the average mixing ratio drops from 40 ppb to 33 ppb (Fig. 5c). Similarly, at the ski resort site of Valle Nevado, which shows  
230 concerning levels of more than 60 ppb of O<sub>3</sub> on average in the baseline case, the mixing ratio drops to an almost constant value of 33 ppb and does not go above 43 ppb. This points to O<sub>3</sub> in Valle Nevado being almost exclusively attributable to Santiago emissions. To a lesser extent, the village of San Gabriel shows the same trend although the still wide distribution in scenario SC advocates for a significant contribution of local sources as well. The impact of Santiago emissions in the vicinity of the Maipo summit is small but remains significant with a decrease by 4 ppb of the daily maxima and average mixing ratios. Given  
235 the nature of the locations Valle Nevado and Maipo, the narrow distribution of O<sub>3</sub> hourly mixing ratio, averaging at 33 ppb and ranging between 25 ppb and 40 ppb, recovered in scenario SC for those sites is indicative of the background concentration for the region, i.e. the distribution of O<sub>3</sub> mixing ratio that would be observed at a site not influenced by anthropogenic emissions.

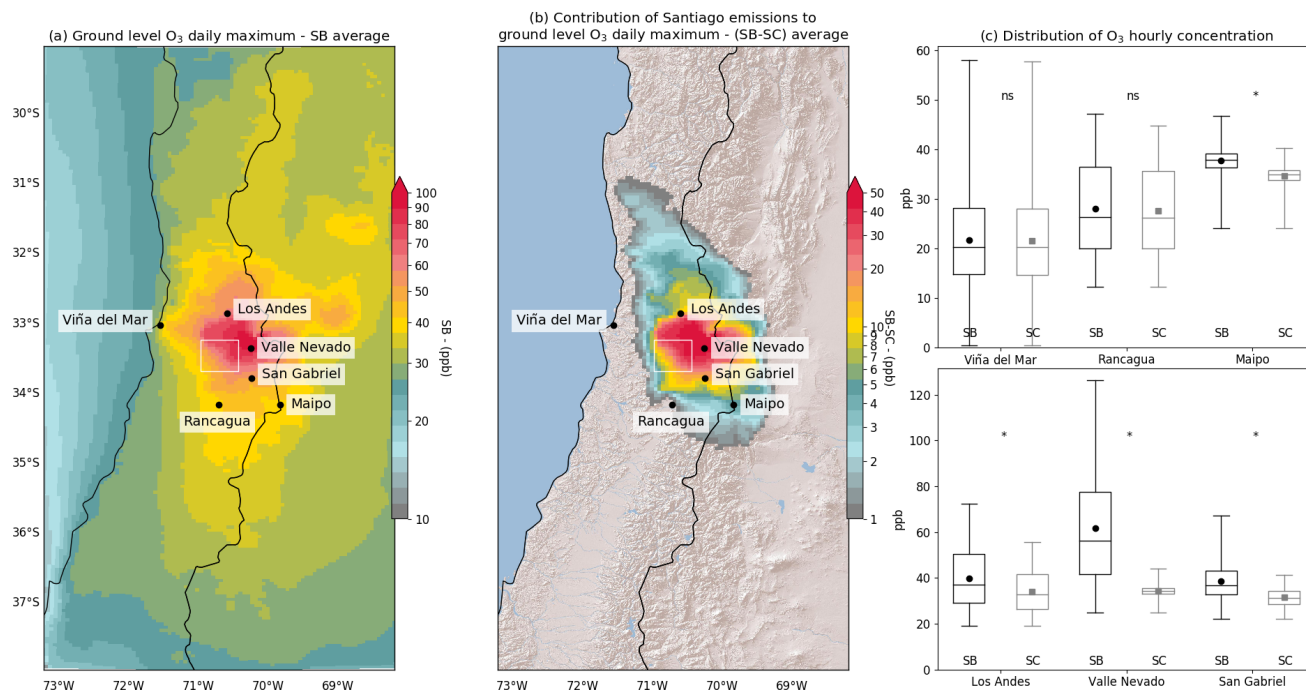


**Figure 5.** (a) Ground-level O<sub>3</sub> average daily maximum of hourly mixing ratio in scenario SB, (b) Difference between SB and SC in ground-level O<sub>3</sub> average daily maximum of hourly mixing ratio. Map background layer: World Shaded Relief, ©2009 ESRI, (c) Distribution of hourly O<sub>3</sub> mixing ratio at six locations in scenario SB (black) and SC (gray) - horizontal lines are quartiles, whiskers show minimum and maximum, dots show the average. "ns" indicates that the distribution in the SB and SC scenarios cannot be distinguished at the 90% level based on a t-test. "\*" indicates that they are different at the 99% level based on that same t-test.

On the other hand, the western and southern areas adjacent to Santiago are barely sensitive to its emissions. In Figure 5c, the distribution of hourly O<sub>3</sub> mixing ratio at Viña del Mar and Rancagua is nearly the same in both scenarios, except for the maximum at Rancagua which is a few ppb lesser in scenario SC than SB. For those two locations, the difference in O<sub>3</sub> distribution with or without Santiago emissions is not significant at the 90% level, while for all other locations, distributions are significantly different at the 99% level.

Regarding the regional transport of PM<sub>2.5</sub> in summertime, the plume shows a similar extent to O<sub>3</sub> in summertime, i.e. an area of influence lesser than in wintertime near the surface (not shown here). O<sub>3</sub> is barely produced in wintertime due to a zenith angle of the sun closer to the horizon and shorter duration of days, resulting in less radiative power and barely active photolysis, so that the question of the export of its precursors at that season is less relevant.

### 3.2 Contribution of regional emissions to atmospheric composition in Santiago

Similarly to the previous approach, we can, in a symmetric manner, deduce the contribution of transport from remote sources to atmospheric composition in the Santiago Metropolitan Area. This is achieved by looking at concentrations in the contribution



250 case, that exclusively originate from non-local sources. Hereafter the analysis focuses again on  $\text{PM}_{2.5}$  in wintertime and  $\text{O}_3$  in summertime.

### 3.2.1 Wintertime $\text{PM}_{2.5}$

Figure 4b indicated that local emissions largely dominate the wintertime  $\text{PM}_{2.5}$  signal for Santiago, with 50% to 100% of the mean surface concentration of  $\text{PM}_{2.5}$  originating locally within the white rectangle. Nevertheless, the contribution of transport  
255 is also significant although heterogeneous in Santiago. Figure 6a shows that in the baseline scenario, the northern and western parts of Santiago feature higher levels of  $\text{PM}_{2.5}$ , with average concentrations ranging between  $30 \mu\text{g m}^{-3}$  and  $100 \mu\text{g m}^{-3}$  for the whole metropolis. In the contribution scenario (Fig. 6b), this pattern is partly recovered, with a smoother gradient from west to east. The underlying conclusion is twofold. First, the transport of pollutants in Santiago mostly comes from the west, which is consistent with the presence of the cordillera in the east not featuring many sources of pollution, and the dominant  
260 westerly daytime wind direction in wintertime. Second, the districts of Santiago facing the worst air quality are also the ones where the transport of pollutants is larger.

However, the differing patterns between Fig. 6a and 6b also shows that local sources in these districts are also stronger. If emissions were similar, the observed gradient in WB would be closer to that in WC. Consistently with this observed westward gradient, we define 5 zones of interest, comprising 6 grid points each along a meridional axis (rectangles and dots in Fig. 6b).  
265 This arrangement ensures that most of the city is covered while maintaining the west-east variability. For each zone we look at the distribution of  $\text{PM}_{2.5}$ , averaged over the 6 grid points, in scenarios WB and WB-WC (Fig. 6c) and WC (Fig. 6d). When averaged meridionally, the westward gradient is also obtained in scenario WB, and conserved when the contribution of transport is subtracted (WB versus (WB-WC) in Fig. 6c). On average, the contribution of transport to  $\text{PM}_{2.5}$  concentration ranges between  $10 \mu\text{g m}^{-3}$  for the westernmost area and  $5 \mu\text{g m}^{-3}$  for the easternmost part, with a monotonic spatial variation  
270 (Fig. 6d). However, this amount always corresponds to 13% to 15% of the WB concentrations. This number is well in line with Barraza et al. (2017) that found 9% of  $\text{PM}_{2.5}$  in Santiago coming from coastal sources, for the period 2011-2012. It is worth noting that given the observed westward gradient, we also recover that coastal sources are likely the main contributor to imported  $\text{PM}_{2.5}$ . Again, transport is larger in western Santiago, and can sporadically reach up to  $30 \mu\text{g m}^{-3}$ , but does not constitute a greater share than in the east.

275 This averaged picture provides a first clue as to the main origin of  $\text{PM}_{2.5}$  transport of Santiago but the picture can be refined by looking at the joint distribution of hourly wind direction and  $\text{PM}_{2.5}$  concentrations as shown in Fig. 7. At the selected southeastern location, mostly clean air comes from the east, i.e. from the Andes where pollutants sources are scarce (less than  $5 \mu\text{g m}^{-3}$  for almost every hour), while winds blowing from the southwest can transport concentrations as high as more than  $20 \mu\text{g m}^{-3}$  for some hours, pointing to the southern cities of Rancagua or San Fernando mentioned previously, or  
280 the southwestern urban location of Melipilla ( $33.6^\circ\text{S}, 71.2^\circ\text{W}$ ). At the northeastern site, winds mainly come from the north where only a handful of urban areas are found, hence leading to a transport seldom exceeding  $10 \mu\text{g m}^{-3}$ . In the center of the metropolitan area, winds are either southwesterlies (from the Rancagua and Melipilla areas) or northwesterlies (from the Viña

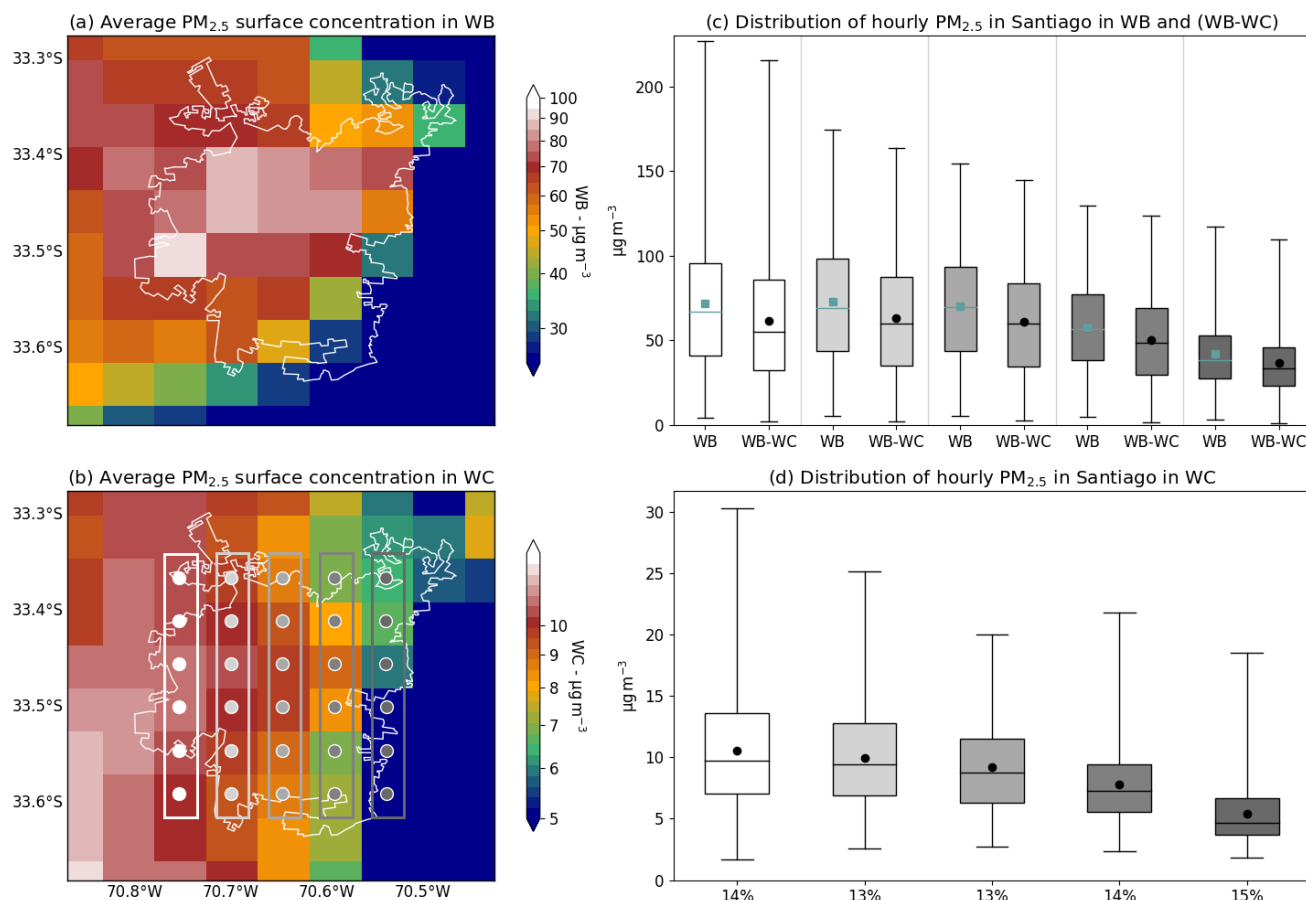


**Figure 6.** (a) Average ground-level PM<sub>2.5</sub> concentration in scenario WB. White contour shows the limits of the Santiago Metropolitan Area. (b) same as (a) for scenario WC, (c) Distribution of hourly PM<sub>2.5</sub> surface concentration in WB and (WB-WC). Boxes show the average, median, minimum, maximum, first and third quartiles. Shades of gray correspond to the zones defined in (b) on which an average is made, (d) same as (c) for scenario WC. Percentages indicate the relative average contribution of transport.

del Mar-Valparaíso area), with both cases leading to similar amounts of imported PM<sub>2.5</sub> mostly above 10 μg m<sup>-3</sup>, i.e. above average. The picture is similar for the northwestern and southwestern sites although wind directions are shifted.

285 In the northwest, center and northeast, the dominant wind directions also coincide with higher maximum relative contributions  
 of transport over the period along these directions (black diamonds in Fig. 7). Sporadically, significant transport events can  
 also come from less frequently observed directions. The maximum relative contribution obtained for the northwest point when  
 winds are from NNE is 75% for example, while such winds occur less than 1% of the time. For southwest and southeast  
 locations, these maximum relative transport episodes are observed when winds blow from the south, in particular in the  
 290 southeast where it can reach up to 100%.

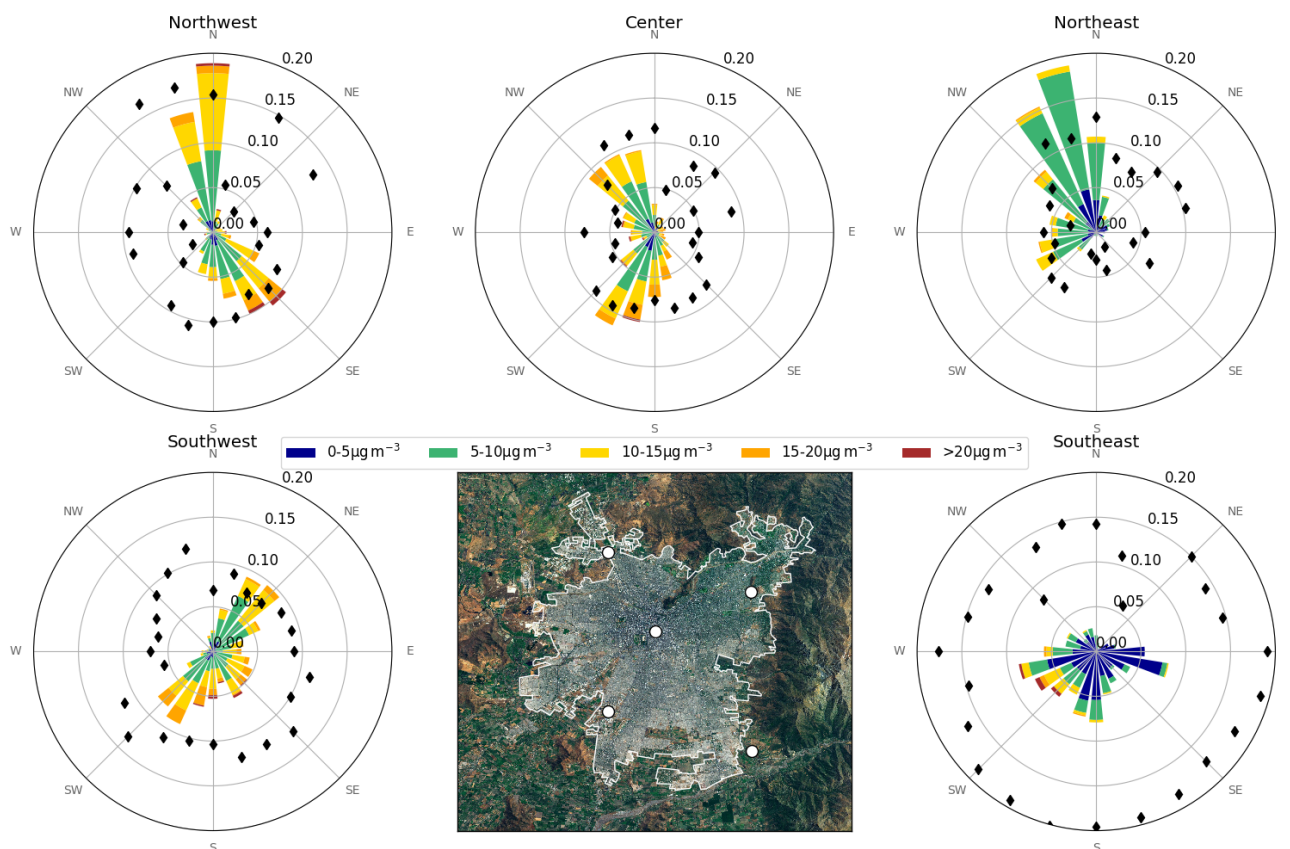


**Figure 7.** Joint distribution of hourly wind direction (length of bar gives the frequency of the corresponding wind direction) and  $\text{PM}_{2.5}$  concentration (colormap) in scenario WC for 5 locations in Santiago. Black diamonds show the maximum relative contribution of transport (i.e. WC/WB) for each wind direction bin (NB: the scale is the wind frequency scale multiplied by 5, i.e. 0.20 is actually 1.0). The bottom center map shows the location of the considered grid points. Map background layer: Imagery World 2D, ©2009 ESRI.

In summary, wintertime  $\text{PM}_{2.5}$  concentrations in Santiago are significantly ( $5 \mu\text{g m}^{-3}$  to  $10 \mu\text{g m}^{-3}$  on average) and always (at least  $1 \mu\text{g m}^{-3}$  for every hour) affected by transport, with identifiable origins, and although the different districts are not equally affected in absolute value, the relative burden of imported particulate matter is equivalent.

### 3.2.2 Summertime $\text{O}_3$

295 Based on the same approach, we find that the summertime transport of  $\text{NO}_x$  within the Santiago basin never exceeds 0.5 ppb, while average values in the SB scenario are between 5 ppb and 40 ppb, with a similar westward gradient as observed for  $\text{PM}_{2.5}$  (not shown here). At the 90% level,  $\text{NO}_x$  transport is thus not significant. Similarly, the transport of VOC is homogeneous over the whole basin at 2 ppb on average, while between 20 ppb and 60 ppb in the SB scenario, which is again not significant at the 90% level. Santiago is thus not affected by the transport of  $\text{O}_3$  precursors.



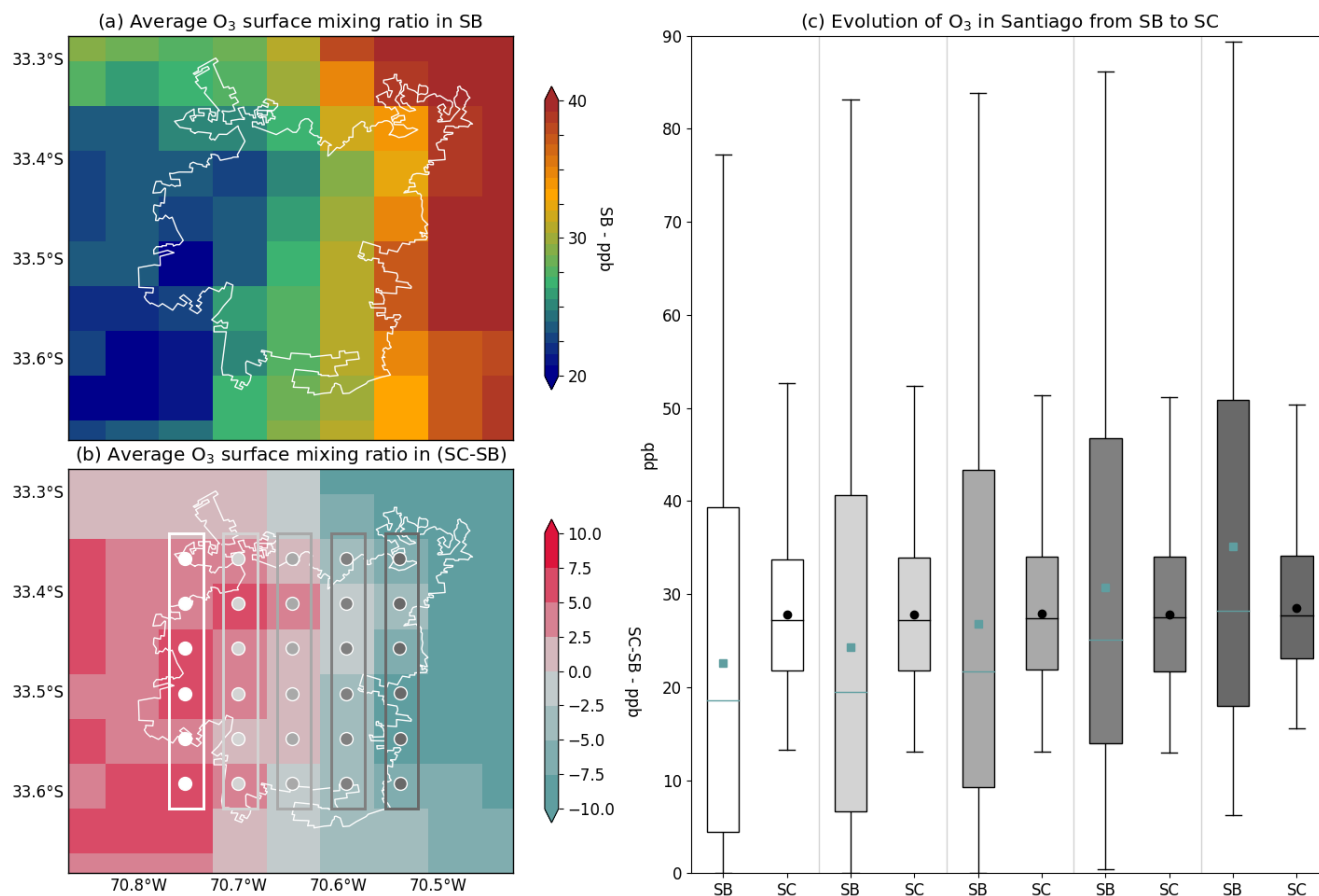
300 However, the picture within the Metropolitan Area in SB and SC scenarios is complex. In the baseline scenario, the eastern  
area of Santiago is more affected by  $O_3$  pollution compared to the western area (Fig. 8a and 8c), consistently with observations  
and the literature (e.g. Menares et al., 2020), due to a more balanced VOC/ $NO_x$  ratio than in the western area. At Independencia  
(center Santiago), the VOC/ $NO_x$  ratio at emission is between 1:1 and 2:1 on average. Contrarily, at Las Condes (eastern  
Santiago) the VOC/ $NO_x$  ratio at emission is around 6:1 on average, in the baseline case (not shown here). A typical  $O_3$   
305 formation ridge line of the VOC/ $NO_x$  concentration ratio in urban areas is around 6:1 to 8:1 (e.g. National Research Council,  
1991; Sillman, 1999), so that Independencia features a VOC-limited regime, while Las Condes features a balanced regime  
favorable to  $O_3$  formation, hence the larger amounts found at the latter location.

Figure 8b shows the consequences, on  $O_3$  surface mixing ratio, of eliminating emissions within Santiago. Given the configuration  
described previously, in the baseline case, the VOC-limited districts of western Santiago feature mixing ratios well below the  
310 background level due to the titration of  $O_3$  by excess quantities of  $NO_x$ , while the eastern districts feature mixing ratios above  
the atmospheric background level due to excess  $O_3$  formation under a favorable regime. As a result of shutting off emissions,  
given that there is no import of precursors as evidenced above, the whole area is set to the background  $O_3$  level of around  
30 ppb described in Section 3.1.2, since there is no influence of anthropogenic pollutants anymore. Therefore, this corresponds  
to an increase (decrease, respectively) of  $O_3$  in western (eastern, respectively) Santiago, thus explaining the dipole obtained  
315 in Figure 8b. Such an evolution is also clear in the evolution of the distribution of hourly  $O_3$  mixing ratios across the city  
between scenario SB and SC (Fig. 8c). While in scenario SB the distribution is shifted towards larger mixing ratios when  
going eastward, in scenario SC all distributions are equal (significant at the 99% level). The leveling of mixing ratios, with no  
gradient across the metropolitan area in scenario SC constitutes an additional evidence that  $O_3$  in Santiago is not affected by  
long-range transport, otherwise heterogeneous patterns similar to what is observed in Figure 6b would be obtained.

### 320 3.3 Advection processes

As discussed around Figure 3 and observed in Figure 4 and Figure 5, advection patterns of pollutants differ between wintertime  
and summertime. So far, the analyses focused on surface fields, but processes along the vertical drive these differences.  
Figure 9 shows an average latitude/altitude transect, along central Chile, of winds, afternoon mixing layer height and pollutants  
concentrations for the corresponding season, in the baseline scenario and the Santiago isolated contribution case.

325 In wintertime (Fig. 9b and 9c), the boundary layer (solid white line) is shallow, and average winds in the FT are strong,  
consistently with the observed semi-permanent inversion layer in the region. As a result, the  $PM_{2.5}$  emitted in large amounts  
mostly remain trapped within this shallow mixing layer. Injection of polluted air masses into the lower FT can also occur,  
through mountain venting, as described in Lapere et al. (2021), explaining why residual concentrations of 1 to 5  $\mu g m^{-3}$  are  
observed higher up in the baseline and contribution scenarios at the latitude of Santiago (Fig. 9b and 9c). Nevertheless, the  
330 long-range export of  $PM_{2.5}$  from Santiago observed in Figure 4 is mainly driven by advection within the boundary layer,  
close to the ground, by weak winds, as evidenced by Figure 9c. Except for a shallow residual layer located above the average  
afternoon boundary layer, pollutants emitted from Santiago remain within it along the transect from Santiago to Viña del Mar.  
The pattern changes when reaching the seashore however, with significant wind shears lifting the  $PM_{2.5}$  layer above the mixing



**Figure 8.** (a) Average O<sub>3</sub> mixing ratio at ground level in scenario SB in Santiago, (b) same as (a) for scenario (SC-SB), (c) Distribution of hourly O<sub>3</sub> surface mixing ratio in scenario SB and SC. Boxes show the average, median, minimum, maximum, first and third quartiles. Shades of gray correspond to the zones defined in (b) on which an average is made.

layer (rightmost part in Fig. 9c) thus explaining the wide northward extent of Santiago contribution, due to transport higher up,  
 335 by intense southerlies.

Interestingly, the summertime transect of O<sub>3</sub> shows a sharp maximum near the latitude of Santiago, several hundred meters above the ground. Figure 9d shows the formation of an O<sub>3</sub> bubble of more than 50 ppb on average, i.e. 15 ppb above the 35 ppb background mixing ratio observed in scenario SB (dominant yellow/green levels in altitude in Figure 9d), around latitude 33°S i.e. slightly north of Santiago, above the planetary boundary layer, extending between 1.5 km and 3 km altitudes. This additional  
 340 O<sub>3</sub> plume is mostly attributable to emissions of precursors in Santiago, that account for more than 15 ppb of O<sub>3</sub> on average at the location of the bubble (Fig. 9e), i.e. the background level exceedance. Thus, despite a relatively limited area where precursors from Santiago affect O<sub>3</sub> formation near the ground (Fig. 5b), their impact on the vertical is more dramatic. The process underlying the formation of this significant O<sub>3</sub> bubble clearly departing from the background, is discussed hereafter.





It is also worth noting that even though export of  $O_3$  close to the surface is limited (Fig. 5b), it is more widespread higher up, with a residual layer originating from Santiago emissions of a few ppb extending 2 km vertically and transporting northward in the FT along  $2^\circ$  of latitude (Fig. 9e).

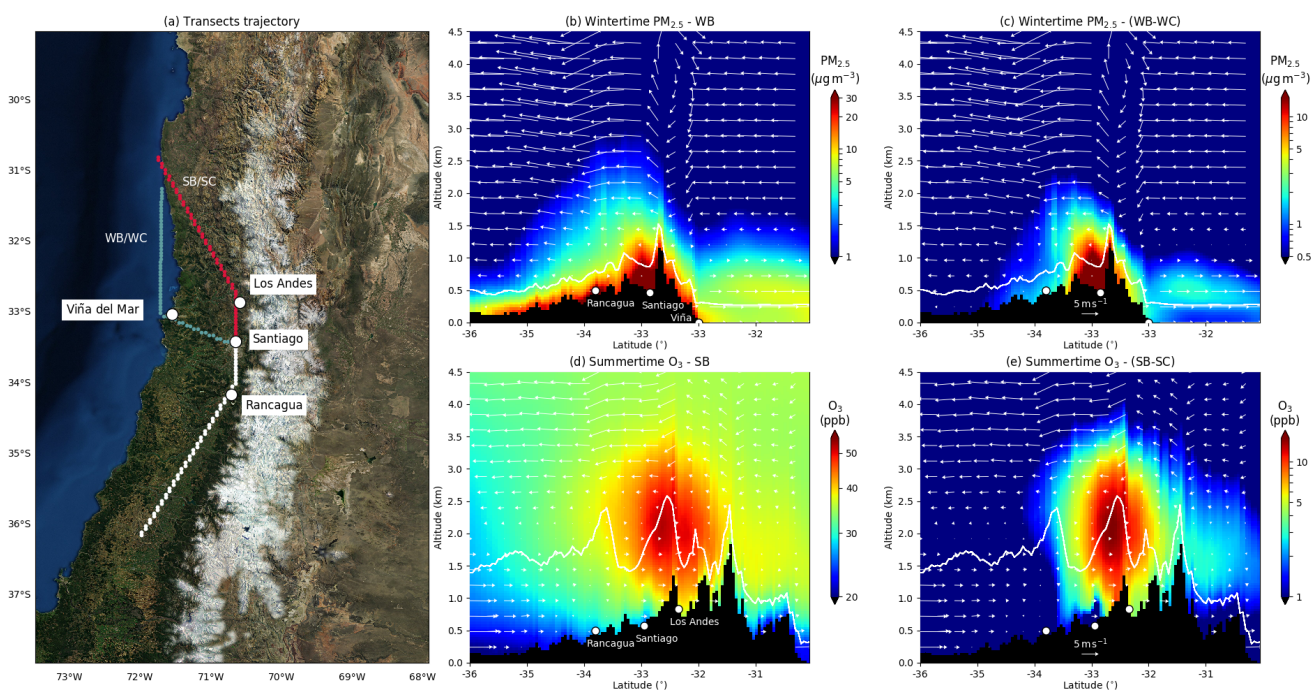


**Figure 9.** (a) Trajectory of the considered latitude/altitude transects and main locations along the way. White dotted line up to Santiago is common for both seasons, blue dotted line is for wintertime, red dotted line for summertime. Values in the transects are not zonally averaged, they correspond to the grid points represented with dots. Map background layer: Imagery World 2D, ©2009 ESRI, (b) Simulated  $PM_{2.5}$  concentrations (colormap), wind (white arrows), afternoon boundary layer (white solid line) and terrain elevation (black area), along the white/blue transect. Average for wintertime 2015 - WB scenario. (c) same as (b) for scenario (WB-WC), (d) Simulated  $O_3$  mixing ratios (colormap), wind (white arrows), afternoon boundary layer (white solid line) and terrain elevation (black area), along the white/red transect. Average for summertime 2015 - SB scenario. (e) same as (d) for scenario (SB-SC).

Given the proximity of the Andes cordillera to the Santiago basin, the formation of the aforementioned  $O_3$  bubble finds its origin in the mountain-valley circulation and the associated mountain venting mechanism. Daytime upslope winds, strong in summertime, lift polluted air masses from the atmospheric boundary layer (ABL) over Santiago into the lower FT, possibly above another location depending on the FT winds direction. McKendry and Lundgren (2000) and Lu and Turco (1996) find that this process is a net sink for boundary layer  $O_3$  in British Columbia and the Los Angeles basin, respectively. Henne et al. (2005) find that the effect of venting in an Alpine environment on FT  $O_3$  concentrations strongly depends on initial mixing ratios within the vented ABL, with either net production if ABL mixing ratios of  $O_3$  are high (urban valleys), or net loss if they are low (remote valleys). However, our study case falls into none of the aforementioned. Such a bubble of  $O_3$ , detached



355 from the ground, with a mixing ratio much higher than at ground level is not found in the literature to our knowledge. More moderate injections, with  $O_3$  mixing ratios lower to similar to surface levels are usually observed. In our case, we find that the venting of precursors from the Santiago polluted ABL leads to the net production of large quantities of  $O_3$  in the FT, larger than at the surface. Schematically, there is a larger export of VOC than  $NO_x$  in the FT (Fig. A3a and A3b) which makes for a balanced chemical regime (below 0.5 is  $NO_x$ -limited, above 0.5 is  $NO_x$ -rich) at around 0.5 at 2 km altitude, while the regime is  
360 close to 1 near the surface hence unfavorable to  $O_3$  production, along the whole transect, due to dominant urban  $NO_x$  emissions (Fig. A3c). Also, the export of Peroxyacetyl nitrate (PAN), which is a  $NO_x$  carrier, into the FT, contributes to enhanced  $O_3$  formation (Fig. A3d).

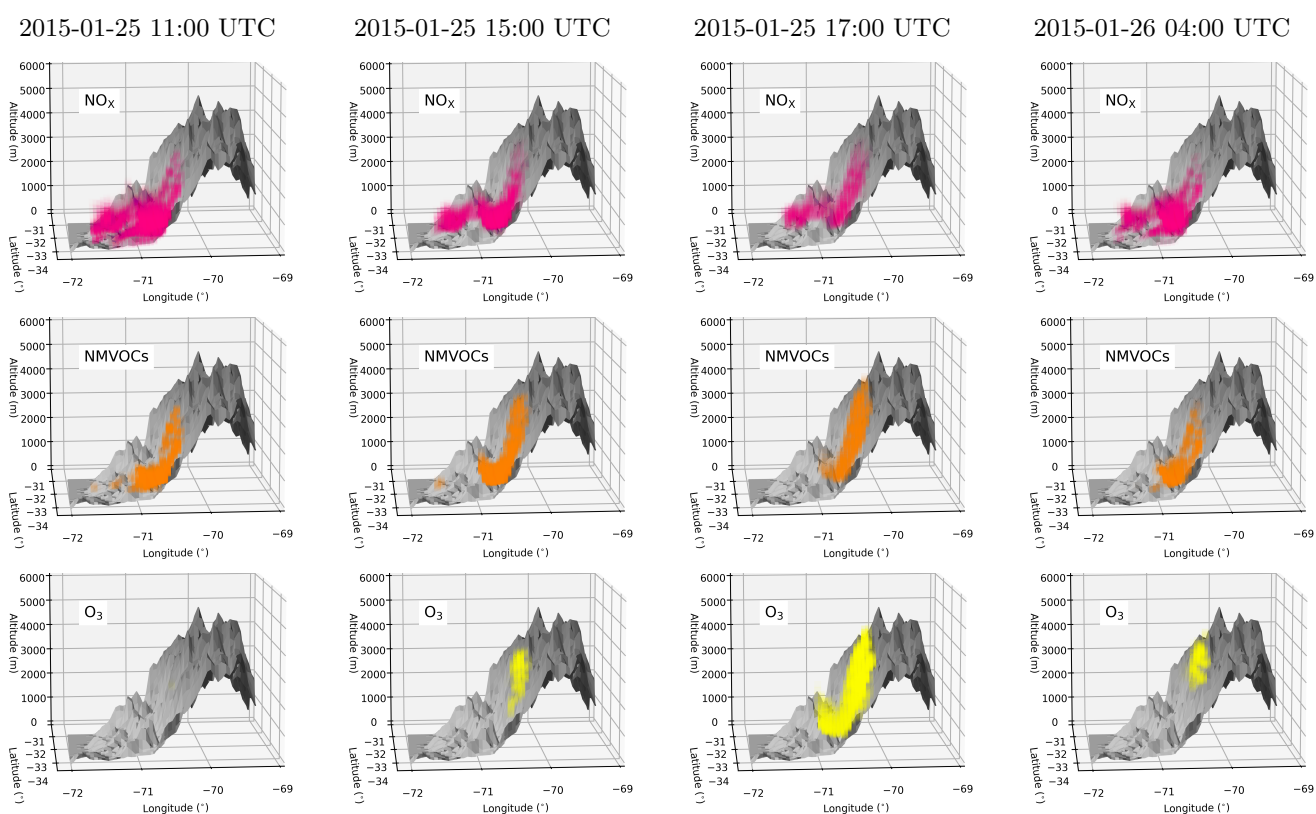


**Figure 10.** Cycle of  $NO_x$  (top), NMVOC (middle) and  $O_3$  (bottom) venting in the vicinity of Santiago for a typical day in January 2015. Hourly mixing ratios in excess of 2 ppb, 20 ppb and 60 ppb are shown, respectively. Each panel shows a 3-dimensional view from a longitudinal perspective. Gray surfaces represent the terrain topography. Santiago is UTC-3 for this period.

Figure 10 further sheds light on the dynamics of this mechanism. Early in the day, at 11:00 UTC (Chile is UTC-3 in summertime), both  $NO_x$  and NMVOC (non-methane VOC) are highly concentrated near the ground (morning peak of emissions  
365 from traffic), and start ascending the Andean foothills, but no  $O_3$  is formed in the region given that sunlight is not intense yet



(leftmost column in Fig. 10). A few hours later, at 12:00 LT (15:00 UTC), the precursors have a similar distribution as in early morning, but the photolysis starts taking place and O<sub>3</sub> is created at the top of the precursors plume, well above the ground.

Two factors explain that O<sub>3</sub> is not formed near the source of precursors. First, given the urban environment of the basin, NO<sub>x</sub> are emitted in large quantities so that the VOC/NO<sub>x</sub> ratio is adverse to neutral, and O<sub>3</sub> is formed in small amounts (see the related discussion in Sect. 3.2.2). But NO<sub>x</sub> have a lifetime much shorter than most VOC (e.g. Monod et al., 2001; Laughner and Cohen, 2019), and when the polluted air parcels are lifted up, the ratio becomes more balanced as NO<sub>x</sub> is consumed closer to the ground. Due to these asymmetric lifetimes and hence export, at some point on the vertical the ratio becomes favorable (Fig. A3c) and O<sub>3</sub> is formed in large quantities. The second factor comes from the increase of photolysis rates with altitude. Several hundred meters above the ground, near or above the mixing layer, photolysis rates of NO<sub>2</sub> are much faster than at ground level (e.g. Pfister et al., 2000) hence favoring the formation of O<sub>3</sub>, all other things being equal. In our simulation, on average, the photolysis of NO<sub>2</sub> is 20% faster 1000 m above ground than at the surface. Also, Figure 9d shows that at the point where the O<sub>3</sub> plume is denser, winds are weak to null on average, so that precursors stagnate, again allowing for more O<sub>3</sub> creation.

At 14:00 LT (17:00 UTC), the vertical export of precursors is even more important due to the maximum development of the deep mixing layer and the full intensity of upslope winds, with two main consequences. First, NO<sub>x</sub> levels in Santiago decrease compared to VOC due to vertical export earlier in the day, leading to a more favorable ratio and O<sub>3</sub> starts forming in the urban basin near the surface. Thus, ventilation of precursors possibly increases O<sub>3</sub> surface concentration in Santiago. Second, the O<sub>3</sub> plume in the lower FT intensifies and extends up to an altitude of 4 km. Finally, at 01:00 LT (04:00 UTC) the next day, the return of a shallower mixing layer and the accumulation of evening traffic emissions make precursors concentrations larger near the ground again. Sun being down, O<sub>3</sub> stops forming, but given the large amounts created during the day, a residual plume remains around 1 km above ground. In parallel, winds along the transect being mostly southerlies, the O<sub>3</sub> plume ends up approximately 50 km north of the Santiago basin.

In addition to being a pollutant, tropospheric O<sub>3</sub> is a strong greenhouse gas, estimated to contribute between 0.2 to 0.6 W m<sup>-2</sup> to present climate global radiative forcing (Myhre et al., 2013). The process described above may then imply radiative effects, either directly through greenhouse effect, indirectly through its impact on moisture, clouds and atmospheric circulation, or through its interaction with the cycles of other greenhouse gases (Mohnen et al., 1993). Estimating this impact is however not in the scope of the present work. Nevertheless, it shows that although the venting of pollutants can be beneficial from the urban air pollution perspective, longer-term effects on climate are a corollary worth investigating.

#### 4 Discussion

Only one particular month per season, for one particular year, are analyzed here. Whether the results presented can be extrapolated with a climatological relevance is not straightforward. Climate variability modes such as ENSO, for instance, can lead to inter-annual changes in circulation and meteorology at the scale of central Chile. However, although our quantitative conclusions may not exactly hold for other years, the underlying processes described remain valid, particularly when it comes to



mountain-valley circulation which is radiatively driven. Variations in primary pollutants and precursors emissions, wintertime  
400 precipitation and cloud cover may affect our results, but we do not expect new processes to take place or evidenced processes  
to stop, nor magnitudes to change entirely.

Section 3.3 evidences the asymmetric vertical ventilation of pollutants such as  $\text{NO}_x$  and VOC and its role in the formation of  
an  $\text{O}_3$  persistent plume. Given the quite unique combination of very high emission rates and close proximity of steep elevated  
orography featured by the Santiago basin, it is unclear, based on the literature, whether this venting is expected to improve  
405 or worsen  $\text{O}_3$  pollution at the surface level in the city. To some extent, this asymmetric venting of precursors is similar to the  
sensitivity analysis performed in Section 3.2 leading to a change in precursors ratios, except for the magnitude of the variation  
in pollutants emissions. Thus, one could extrapolate and expect an increase (decrease, respectively) of  $\text{O}_3$  mixing ratio in  
the western (eastern, respectively) districts due to this daily-occurring export of pollutants, compared to a situation where air  
masses would stagnate. However, there are too many non-linear processes involved to be affirmative on this point.

410 Despite our good confidence in the model, it is not possible to strengthen conclusiveness with observations on the newly  
evidenced  $\text{O}_3$  bubble we find as there are no local measurements of  $\text{O}_3$  profiles for our study period. Besides, tropospheric  
ozone column products from satellite data are usually not fit for analysis in mountainous regions (e.g. Kar et al., 2010).  
However, Seguel et al. (2013) conducted ozone profile measurements in the Santiago region in summer 2011 that match our  
results quite well. First, they find a similar 35 ppb free troposphere background  $\text{O}_3$  mixing ratio. Second, they evidence several  
415 occurrences of deep residual layers as intense as 100 ppb of  $\text{O}_3$  slightly north of Santiago (at the location of La Colina, between  
Santiago and Los Andes) in early afternoon, measured between 1.5 km and 2.5 km above ground. Such secondary layers higher  
up are consistent with our findings. If a vertical profile is taken north of Santiago in Fig 9d, a bell shaped profile is recovered,  
of maximum intensity near 2 km above ground, much like Figure 9 in Seguel et al. (2013). Thus, our simulation results agree  
very well with the measurements conducted in Seguel et al. (2013), despite being for a different year, hence strengthening  
420 our conclusions on the existence of the newly evidenced  $\text{O}_3$  bubble and its seasonal persistence. Similarly to our findings,  
Seguel et al. (2013) also concluded that the residual layer is coming from pollutants venting from Santiago. However their  
measurement-based approach did not allow to evidence (i) the exact formation mechanism of this bubble, (ii) its persistent  
character even through nighttime (measurements presented are only for daytime), (iii) its horizontal extent (measurements are  
discrete in space). Our modeling approach based on sensitivity analysis confirms the primary role of Santiago emissions and  
425 gives a clearer and continuous 3-dimensional picture of the phenomenon, while agreeing with the findings of these previous  
measurements.

We estimate that 14% of  $\text{PM}_{2.5}$  in Santiago come from long-range transport in wintertime. Although summertime  $\text{PM}_{2.5}$  is  
not discussed within the framework of this paper, it is available in the simulations, and we find its transported contribution to  
be greater, at 22%, for that period. As a result, we expect the average contribution of long-range transport to  $\text{PM}_{2.5}$  in Santiago  
430 for a whole year to be somewhere between these two numbers, around 18%. It is worth noting that for the year 2019, the  
exceedance of the  $\text{PM}_{2.5}$  Chilean standard was 18% for Santiago according to data from the SINCA network. Although for our  
study year 2015 this exceedance was higher (close to 50%), our findings suggest that if air quality improvement policies are

conducted in all urban areas across central Chile, Santiago might be able to meet the national standards more easily due to the large contribution of transported  $PM_{2.5}$ .

## 435 5 Conclusions

Based on chemistry-transport modeling with WRF-CHIMERE, the present work investigates the transport of atmospheric pollutants in central Chile for one winter month and one summer month. Our findings show that emissions of the Santiago Metropolitan Area greatly affect atmospheric composition in its vicinity and farther, with a contribution of a few  $\mu\text{g m}^{-3}$  to  $PM_{2.5}$  in wintertime corresponding to 5% to 10% of surface concentrations as far as  $4^\circ$  north and  $4^\circ$  south. This transport is  
440 mostly driven by surface winds within the boundary layer above land, and takes place in the free troposphere over the ocean hence explaining its long northward range. The spatial extent of the effect on surface concentrations of  $O_3$  precursors emitted in Santiago in summertime is lesser. Nevertheless, daily peaks of  $O_3$  in the direct vicinity of Santiago are reduced by up to 50 ppb on average when emissions from the metropolitan area are eliminated. Conversely, the contribution of long-range transport of  $PM_{2.5}$  in wintertime is responsible for  $5 \mu\text{g m}^{-3}$  to  $10 \mu\text{g m}^{-3}$  on average in downtown Santiago, corresponding to  
445 around 14% of the baseline concentration. While the transport of  $O_3$  precursors to Santiago in summertime is not significant, if emissions of precursors were to be decreased in the city, its western districts would see their  $O_3$  mixing ratios increase on average, despite daily peaks largely dropping, while the eastern area would improve for every quantile. This phenomenon is linked to heterogeneous emissions within the city, which make for currently higher (lower, respectively) than background levels in the east (the west, respectively). When all emissions are cut, the whole area is brought to background, hence the  
450 respective variations. The vertical export of precursors above Santiago in summertime, in relation with unperturbed mountain-valley circulation and venting, creates a persistent  $O_3$  bubble of more than 50 ppb on average, around 1000 m above the ground, slightly north of the city. Daytime upslope winds, the heterogeneous lifetimes of precursors, and increasing vertical profiles of photolysis rate account for this formation, which impact should be looked at in greater detail in terms of surface air quality improvement (or worsening), and photo-chemical and greenhouse effects.

455 *Code availability.* The CHIMERE model used can be found at <http://www.lmd.polytechnique.fr/chimere/CW-download.php> (last access 1 December 2020). The WRF model used can be found at [http://www2.mmm.ucar.edu/wrf/users/download/get\\_source.html](http://www2.mmm.ucar.edu/wrf/users/download/get_source.html) (last access 1 December 2020).

*Data availability.* Surface observation data used in this study are available at <https://sinca.mma.gob.cl/index.php/region/index/id/M> (last access 1 December 2020). HTAP raw emission inventory can be downloaded at [http://edgar.jrc.ec.europa.eu/htap\\_v2/](http://edgar.jrc.ec.europa.eu/htap_v2/) (last access 1 December  
460 2020). Other data can be made available from the corresponding author upon reasonable request.



*Author contributions.* LM and SM supervised the chemistry transport simulations and analysis of the results. NH participated in the critical analysis of the results. RL performed the conceptualization, data analysis and model simulations, and coordinated the writing of the paper with LM, SM and NH.

*Competing interests.* The authors declare that they have no conflict of interest.

465 *Acknowledgements.* The chemistry-transport simulations used in this work were performed using the high-performance computing resources of TGCC (Très Grand Centre de Calcul du CEA) under the allocation GEN10274 provided by GENCI (Grand Équipement National de Calcul Intensif).



## References

- Barraza, F., Lambert, F., Jorquera, H., Villalobos, A. M., and Gallardo, L.: Temporal evolution of main ambient PM<sub>2.5</sub> sources in Santiago, Chile, from 1998 to 2012, *Atmos. Chem. Phys.*, 17, 10 093–10 107, <https://doi.org/10.5194/acp-17-10093-2017>, 2017.
- Chung, S. H. and Seinfeld, J. H.: Climate response of direct radiative forcing of anthropogenic black carbon, *J. Geophys. Res.*, 110, D11 102, <https://doi.org/10.1029/2004JD005441>, 2005.
- de la Barrera, F., Barraza, F., Favier, P., Ruiz, V., and Quense, J.: Megafires in Chile 2017: Monitoring multiscale environmental impacts of burned ecosystems, *Sci. Total Environ.*, 637-638, 1526–1536, <https://doi.org/10.1016/j.scitotenv.2018.05.119>, 2018.
- 475 Dominutti, P., Nogueira, T., Fornaro, A., and Borbon, A.: One decade of VOCs measurements in São Paulo megacity: Composition, variability, and emission evaluation in a biofuel usage context, *Sci. Total Environ.*, 738, 139 790, <https://doi.org/10.1016/j.scitotenv.2020.139790>, 2020.
- Friedl, M. A., Sulla-Menashe, D., Tan, B., Schneider, A., Ramankutty, N., Sibley, A., and Huang, X.: MODIS Collection 5 global land cover: Algorithm refinements and characterization of new datasets, 2001-2012, Collection 5.1 IGBP Land Cover, <http://lpdaac.usgs.gov>, 2010.
- 480 Gramsch, E., Cereceda-Balic, F., Oyola, P., and von Baer, D.: Examination of pollution trends in Santiago de Chile with cluster analysis of PM10 and Ozone data, *Atmos. Environ.*, 40, 5464–5475, <https://doi.org/10.1016/j.atmosenv.2006.03.062>, 2006.
- Henne, S., Dommen, J., Neininger, B., Reimann, S., Staehelin, J., and Prévôt, A. S. H.: Influence of mountain venting in the Alps on the ozone chemistry of the lower free troposphere and the European pollution export, *J. Geophys. Res.*, 110, D22 307, <https://doi.org/10.1029/2005JD005936>, 2005.
- 485 Hill, A. C. and Littlefield, N.: Ozone. Effect on Apparent Photosynthesis, Rate of Transpiration, and Stomatal Closure in Plants, *Environ. Sci. Technol.*, 3, 52–56, <https://doi.org/10.1021/es60024a002>, 1969.
- Huneus, N., van der Gon, H. D., Castesana, P., Menares, C., Granier, C., Granier, L., Alonso, M., Andrade, M. F., Dawidowski, L., Gallardo, L., Gomez, D., Klimont, Z., Janssens-Maenhout, G., Osses, M., Puliafito, S. E., Rojas, N., Sánchez-Ccoyllo, O., Tolvett, S., and Ynoue, R. Y.: Evaluation of anthropogenic air pollutant emission inventories for South America at national and city scale, *Atmos. Environ.*, 235, 490 117 606, <https://doi.org/10.1016/j.atmosenv.2020.117606>, 2020.
- Ilabaca, M., Olaeta, I., Campos, E., Villaire, J., Tellez-Rojo, M. M., and Romieu, I.: Association between Levels of Fine Particulate and Emergency Visits for Pneumonia and other Respiratory Illnesses among Children in Santiago, Chile, *J. Air Waste Manage.*, 49, 154–163, <https://doi.org/10.1080/10473289.1999.10463879>, 1999.
- Janssens-Maenhout, G., Crippa, M., Guizzardi, D., Dentener, F., Muntean, M., Pouliot, G., Keating, T., Zhang, Q., Kurokawa, J., Wankmüller, R., Denier van der Gon, H., Kuenen, J. J. P., Klimont, Z., Frost, G., Darras, S., Koffi, B., and Li, M.: HTAPv2.2: a mosaic of regional and global emission grid maps for 2008 and 2010 to study hemispheric transport of air pollution, *Atmos. Chem. Phys.*, 15, 11 411–11 432, <https://doi.org/10.5194/acp-15-11411-2015>, 2015.
- 495 Kar, J., Fishman, J., Creilson, J. K., Richter, A., Ziemke, J., and Chandra, S.: Are there urban signatures in the tropospheric ozone column products derived from satellite measurements?, *Atmos. Chem. Phys.*, 10, 5213–5222, <https://doi.org/10.5194/acp-10-5213-2010>, 2010.
- 500 Koch, D. and Genio, A. D. D.: Black carbon semi-direct effects on cloud cover: review and synthesis, *Atmos. Chem. Phys.*, 10, 7685–7696, <https://doi.org/10.5194/acp-10-7685-2010>, 2010.
- Lapere, R., Menut, L., Mailler, S., and Huneus, N.: Soccer games and record breaking PM<sub>2.5</sub> pollution events in Santiago, Chile, *Atmos. Chem. Phys.*, 20, 4681–4694, <https://doi.org/10.5194/acp-20-4681-2020>, 2020.



- Lapere, R., Mailler, S., Menut, L., and Huneus, N.: Pathways for wintertime deposition of anthropogenic light-absorbing particles on the  
505 Central Andes cryosphere, *Environ. Pollut.*, <https://doi.org/10.1016/j.envpol.2020.115901>, 2021.
- Laughner, J. L. and Cohen, R. C.: Direct observation of changing NO<sub>x</sub> lifetime in North American cities, *Science*, 366, 723–727,  
<https://doi.org/10.1126/science.aax6832>, 2019.
- Lippmann, M.: Health effects of tropospheric ozone, *Environ. Sci. Technol.*, 25, 1954–1962, <https://doi.org/10.1021/es00024a001>, 1991.
- Lu, R. and Turco, R. P.: Ozone distributions over the Los Angeles basin: three-dimensional simulations with the smog model, *Atmos.*  
510 *Environ.*, 30, 4155–4176, [https://doi.org/10.1016/1352-2310\(96\)00153-7](https://doi.org/10.1016/1352-2310(96)00153-7), 1996.
- Mailler, S., Menut, L., Khvorostyanov, D., Valari, M., Couvidat, F., Siour, G., Turquety, S., Briant, R., Tuccella, P., Bessagnet, B., Colette,  
A., Létinois, L., Markakis, K., and Meleux, F.: CHIMERE-2017: from urban to hemispheric chemistry-transport modeling, *Geosci. Model*  
*Dev.*, 10, 2397–2423, <https://doi.org/10.5194/gmd-10-2397-2017>, 2017.
- Marín, J. C., Raga, G. B., Arévalo, J., Baumgardner, D., Córdova, A. M., Pozo, D., Calvo, A., Castro, A., Fraile, R.,  
515 and Sorribas, M.: Properties of particulate pollution in the port city of Valparaíso, Chile, *Atmos. Environ.*, 171, 301–316,  
<https://doi.org/10.1016/j.atmosenv.2017.09.044>, 2017.
- Mazzeo, A., Huneus, N., Ordoñez, C., Orfanoz-Chequela, A., Menut, L., Mailler, S., Valari, M., van der Gon, H. D., Gallardo, L., Muñoz,  
R., Donoso, R., Galleguillos, M., Osses, M., and Tolvet, S.: Impact of residential combustion and transport emissions on air pollution in  
Santiago during winter, *Atmos. Environ.*, 190, 195–208, <https://doi.org/10.1016/j.atmosenv.2018.06.043>, 2018.
- 520 McKendry, I. and Lundgren, J.: Tropospheric layering of ozone in regions of urbanized complex and/or coastal terrain: a review, *Prog. Phys.*  
*Geogr.*, 24, 329–354, <https://doi.org/10.1177/030913330002400302>, 2000.
- Menares, C., Gallardo, L., Kanakidou, M., Seguel, R., and Huneus, N.: Increasing trends (2001–2018) in photochemical activity and  
secondary aerosols in Santiago, Chile, *Tellus B Chem Phys Meteorol*, 72, 1–18, <https://doi.org/10.1080/16000889.2020.1821512>, 2020.
- Menut, L., Vautard, R., Flamant, C., Abonne, C., Beekmann, M., Chazette, P., Flamant, P. H., Gombert, D., Guédalia, D., Kley, D., Lefebvre,  
525 M. P., Lossec, B., Martin, D., Mégie, G., Perros, P., Sicard, M., and Toupance, G.: Measurements and modelling of atmospheric pollution  
over the Paris area: an overview of the ESQUIF Project, *Ann. Geophys.*, 18, 1467–1481, <https://doi.org/10.1007/s00585-000-1467-y>,  
2000.
- Menut, L., Bessagnet, B., Khvorostyanov, D., Beekmann, M., Blond, N., Colette, A., Coll, I., Curci, G., Foret, G., Hodzic, A., Mailler, S.,  
Meleux, F., Monge, J.-L., Pison, I., Siour, G., Turquety, S., Valari, M., Vautard, R., and Vivanco, M. G.: CHIMERE 2013: a model for  
530 regional atmospheric composition modelling, *Geosci. Model Dev.*, 6, 981–1028, <https://doi.org/10.5194/gmd-6-981-2013>, 2013.
- MMA: Análisis General para el Impacto Económico y Social (AGIES) de la Norma de Calidad Primaria de Material Particulado 2.5,  
Tech. rep., Ministerio del Medio Ambiente, [http://planesynormas.mma.gob.cl/archivos/2014/proyectos/235\\_6\\_\\_Folio\\_N\\_881\\_al\\_1008](http://planesynormas.mma.gob.cl/archivos/2014/proyectos/235_6__Folio_N_881_al_1008.pdf).  
pdf, 2012.
- Mohnen, V. A., Goldstein, W., and Wang, W.-C.: Tropospheric Ozone and Climate Change, *Air & Waste*, 43, 1332–1344,  
535 <https://doi.org/10.1080/1073161X.1993.10467207>, 1993.
- Monod, A., Sive, B. C., Avino, P., Chen, T., Blake, D. R., and Rowland, F. S.: Monoaromatic compounds in ambient air of various  
cities: a focus on correlations between the xylenes and ethylbenzene, *Atmos. Environ.*, 35, 135–149, [https://doi.org/10.1016/S1352-2310\(00\)00274-0](https://doi.org/10.1016/S1352-2310(00)00274-0), 2001.
- Myhre, G., Shindell, D., Bréon, F.-M., Collins, W., Fuglestedt, J., Huang, J., Koch, D., Lamarque, J.-F., Lee, D., Mendoza, B., Nakajima, T.,  
540 Robock, A., Stephens, G., Takemura, T., and Zhang, H.: In: *Climate Change 2013: The Physical Science Basis. Contribution of Working*  
*Group I to the Fifth Assessment Report of the Intergovernmental Panel on Climate Change*, chap. Anthropogenic and Natural Radiative





- Forcing, [Stocker, T.F. and Qin, D. and Plattner, G.-K. and Tignor, M. and Allen, S.K. and Boschung, J. and Nauels, A. and Xia, Y. and Bex, V. and Midgley, P.M.], Cambridge University Press, Cambridge, United Kingdom and New York, NY, USA, 2013.
- National Research Council: Rethinking the Ozone Problem in Urban and Regional Air Pollution, The National Academies Press, Washington, DC, <https://doi.org/10.17226/1889>, 1991.
- 545 NCEP: NCEP FNL Operational Model Global Tropospheric Analyses, continuing from July 1999, <https://doi.org/10.5065/D6M043C6>, 2000.
- OECD: The Economic Consequences of Outdoor Air Pollution, Tech. rep., Organisation for Economic Co-operation and Development, <https://doi.org/10.1787/9789264257474-en>, 2016.
- Pfister, G., Baumgartner, D., Maderbacher, R., and Putz, E.: Aircraft measurements of photolysis rate coefficients for ozone and nitrogen dioxide under cloudy conditions, *Atmos. Environ.*, 34, 4019–4029, [https://doi.org/10.1016/S1352-2310\(00\)00149-7](https://doi.org/10.1016/S1352-2310(00)00149-7), 2000.
- 550 Puliafito, S. E., Allende, D. G., Castesana, P. S., and Ruggeri, M. F.: High-resolution atmospheric emission inventory of the argentine energy sector. Comparison with edgar global emission database, *Heliyon*, 3, e00489, <https://doi.org/10.1016/j.heliyon.2017.e00489>, 2017.
- Resquin, M. D., Santágata, D., Gallardo, L., Gómez, D., Rössler, C., and Dawidowski, L.: Local and remote black carbon sources in the Metropolitan Area of Buenos Aires, *Atmos. Environ.*, 182, 105–114, <https://doi.org/10.1016/j.atmosenv.2018.03.018>, 2018.
- 555 Rowe, P. M., Cordero, R. R., Warren, S. G., Stewart, E., Doherty, S. J., Pankow, A., Schrempf, M., Casassa, G., Carrasco, J., Pizarro, J., MacDonell, S., Damiani, A., Lambert, F., Rondanelli, R., Huneeus, N., Fernandez, F., and Neshyba, S.: Black carbon and other light-absorbing impurities in snow in the Chilean Andes, *Sci. Rep.*, 9, 4008, <https://doi.org/10.1038/s41598-019-39312-0>, 2019.
- Rubio, M. A., Lissi, E., Gramsch, E., and Garreaud, R. D.: Effect of Nearby Forest Fires on Ground Level Ozone Concentrations in Santiago, Chile, *Atmosphere*, 6, 1926–1938, <https://doi.org/10.3390/atmos6121838>, 2015.
- 560 Rutllant, J. and Garreaud, R.: Meteorological Air Pollution Potential for Santiago, Chile: Towards an Objective Episode Forecasting, *Environ. Monit. Assess.*, 34, 223–244, <https://doi.org/10.1007/BF00554796>, 1995.
- Saide, P. E., Mena-Carrasco, M., Tolvett, S., Hernandez, P., and Carmichael, G. R.: Air quality forecasting for winter-time PM<sub>2.5</sub> episodes occurring in multiple cities in central and southern Chile, *J. Geophys. Res. Atmos.*, 121, 558–575, <https://doi.org/10.1002/2015JD023949>, 2016.
- 565 Sanhueza, P. A., Torreblanca, M. A., Diaz-Robles, L. A., Schiappacasse, L. N., Silva, M. P., and Astete, T. D.: Particulate Air Pollution and Health Effects for Cardiovascular and Respiratory Causes in Temuco, Chile: A Wood-Smoke-Polluted Urban Area, *J Air Waste Manag Assoc*, 59, 1481–1488, <https://doi.org/10.3155/1047-3289.59.12.1481>, 2012.
- Seguel, R. J., Mancilla, C. A., Rondanelli, R., Leiva, M. A., and Morales, R. G.: Ozone distribution in the lower troposphere over complex terrain in Central Chile, *J. Geophys. Res. Atmos.*, 118, 2966–2980, <https://doi.org/10.1002/jgrd.50293>, 2013.
- 570 Seguel, R. J., Gallardo, L., Fleming, Z. L., and Landeros, S.: Two decades of ozone standard exceedances in Santiago de Chile, *Air Qual Atmos Health*, 13, 593–605, <https://doi.org/10.1007/s11869-020-00822-w>, 2020.
- Seinfeld, J. H. and Pandis, S. N.: *Atmospheric Chemistry and Physics: From Air Pollution to Climate Change*. Second Edition., John Wiley & Sons, Inc., Hoboken, New Jersey, 2006.
- Sillman, S.: The relation between ozone, NO<sub>x</sub> and hydrocarbons in urban and polluted rural environments, *Atmos. Environ.*, 33, 1821–1845, [https://doi.org/10.1016/S1352-2310\(98\)00345-8](https://doi.org/10.1016/S1352-2310(98)00345-8), 1999.
- 575 Skamarock, W. C., Klemp, J. B., Dudhia, J., Gill, D. O., Barker, D. M., Duda, M. G., Huang, X.-Y., Wang, W., and Powers, J. G.: A Description of the Advanced Research WRF Version 3, NCAR Technical Note, 27, 2008.



- 580 Soza, L. N., Jordanova, P., Nicolis, O., Štřelec, L., and Stehlík, M.: Small sample robust approach to outliers and correlation of atmospheric pollution and health effects in Santiago de Chile, *Chemom. Intell. Lab. Syst.*, 185, 73–84, <https://doi.org/10.1016/j.chemolab.2018.12.010>, 2019.
- Toro, R. A., Donoso, C. S., Seguel, R. A., Morales, R. G. E., and Leiva G, M. A.: Photochemical ozone pollution in the Valparaiso Region, Chile, *Air Qual Atmos Health*, 7, 1–11, <https://doi.org/10.1007/s11869-013-0218-7>, 2014.
- 585 Toro, R. A., Kvakić, M., Klaić, Z. B., Koračin, D., Morales, R. G. E., and Leiva G, M. A.: Exploring atmospheric stagnation during a severe particulate matter air pollution episode over complex terrain in Santiago, Chile, *Environ. Pollut.*, 244, 705–714, <https://doi.org/10.1016/j.envpol.2018.10.067>, 2019.
- Vardoulakis, S. and Kassomenos, P.: Sources and factors affecting PM10 levels in two European cities: Implications for local air quality management, *Atmos. Environ.*, 42, 3949–3963, <https://doi.org/10.1016/j.atmosenv.2006.12.021>, 2008.
- Walcek, C. J. and Yuan, H.-H.: Calculated Influence of Temperature-Related Factors on Ozone Formation Rates in the Lower Troposphere, *J. Appl. Meteor.*, 34, 1056–1069, [https://doi.org/10.1175/1520-0450\(1995\)034<1056:CIOTRF>2.0.CO;2](https://doi.org/10.1175/1520-0450(1995)034<1056:CIOTRF>2.0.CO;2), 1995.
- 590 Whiteman, D. C.: *Mountain Meteorology: Fundamentals and Applications*, Oxford University Press, 2000.



## Appendix A: Appendix A

WRF configuration		CHIMERE configuration	
Horizontal resolution	5km	Horizontal resolution	5km
Vertical levels	60	Vertical levels	30
Microphysics	WSM3	Chemistry	MELCHIOR
Boundary and surface layer	MYNN	Gas/Aerosol Partition	ISORROPIA
Land surface	Noah LSM	Horizontal Advection	Van Leer
Cumulus parameterization	Grell G3	Vertical Advection	Upwind
Longwave radiation	CAM	Boundary Conditions	LMDz-INCA + GOCART
Shortwave radiation	Dudhia		

**Table A1.** WRF and CHIMERE configurations.

Station	Wintertime						Summertime					
	Independencia			Rancagua			Independencia			Rancagua		
	MB	NRMSE	R	MB	NRMSE	R	MB	NRMSE	R	MB	NRMSE	R
T2	-1.23	0.22	0.87	-1.65	0.28	0.7	0.4	0.16	0.75	-0.06	0.19	0.73
RH	-0.22	0.39	0.85	-0.17	0.35	0.85	-0.12	0.3	0.83	-0.12	0.4	0.8
U10	-0.11	0.36	0.52	-0.01	0.2	0.77	0.31	0.84	-0.06	0.32	0.75	0.09
V10	-0.03	0.27	0.82	0.28	0.12	0.87	1.09	2.11	0.65	0.03	0.33	0.4

Station	Los Andes						Viña del Mar					
	Los Andes			Viña del Mar			Andacollo			Viña del Mar		
	MB	NRMSE	R	MB	NRMSE	R	MB	NRMSE	R	MB	NRMSE	R
T2	-3.33	0.38	0.89	0.31	0.3	0.25	0.67	0.17	0.8	0.64	0.42	0.18
RH	-0.17	0.3	0.91	-0.17	0.74	0.47	0.0	0.13	0.81	-0.06	0.57	0.51
U10	0.29	0.39	0.77	-0.12	1.35	0.29	0.85	1.36	-0.08	0.83	2.68	0.31
V10	0.74	0.65	0.58	2.12	1.54	0.61	2.14	1.14	0.25	0.96	1.57	0.64

**Table A2.** Simulation scores for daily average low-level meteorology for wintertime and summertime 2015. T2 is the 2 m air temperature ( $^{\circ}\text{C}$ ), RH the surface relative humidity, U10 10 m zonal wind and V10 10 m meridional wind speed ( $\text{m s}^{-1}$ ). MB is the mean bias, NRMSE the normalized root mean square error and R the Pearson correlation coefficient.



Day:	21 July			23 July		
	MB	NRMSE	R	MB	NRMSE	R
TEMP	-0.3	0.03	1.0	1.13	0.07	1.0
RH	-0.17	0.32	0.79	-0.04	0.25	0.48
U	1.29	0.16	0.89	-1.65	0.35	0.56
V	-0.46	0.2	0.82	3.52	0.31	0.83
Day:	24 July			25 July		
	MB	NRMSE	R	MB	NRMSE	R
TEMP	2.36	0.08	1.0	1.15	0.06	1.0
RH	-0.03	0.53	0.01	-0.04	0.17	0.89
U	-0.52	0.14	0.86	-0.51	0.16	0.86
V	0.62	0.13	0.92	3.35	0.29	0.86

**Table A3.** Simulation scores for meteorological vertical profiles for four days in July 2015 at noon local time at Quinta Normal station in Santiago. The same notations as in Table A2 apply.

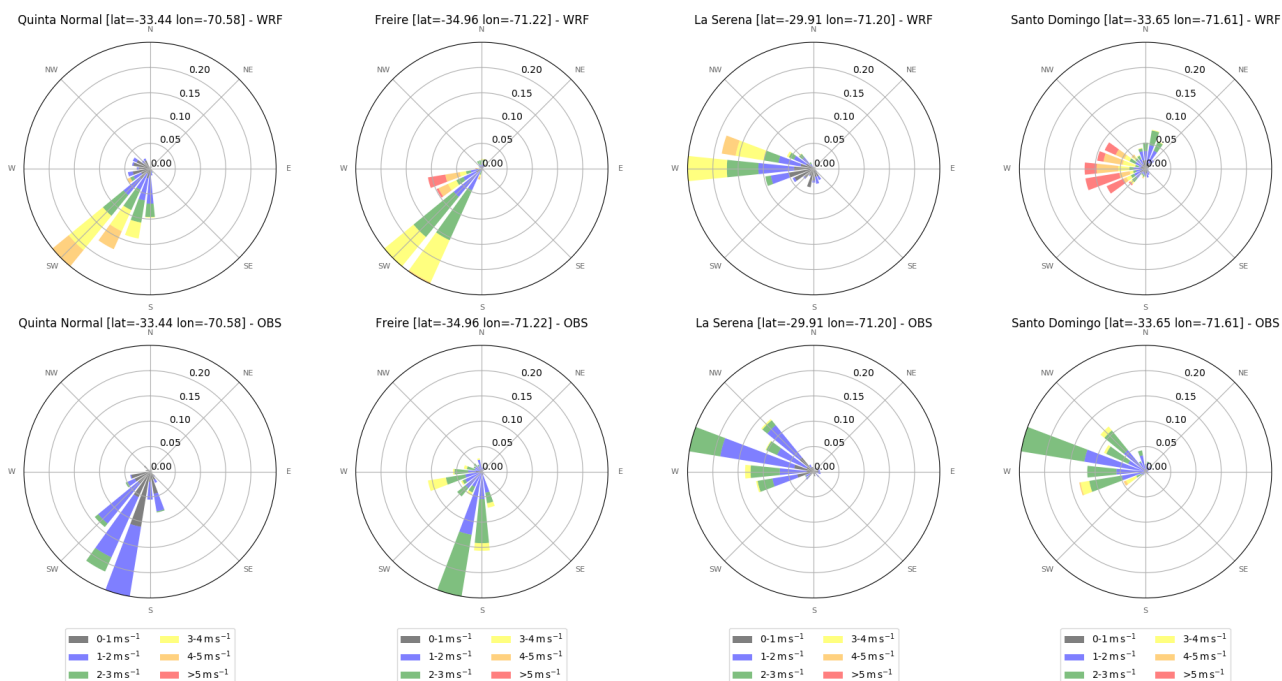


**Figure A1.** 10 m wind distribution in the simulation (top) and observations (bottom) at four locations in central Chile for summertime 2015.

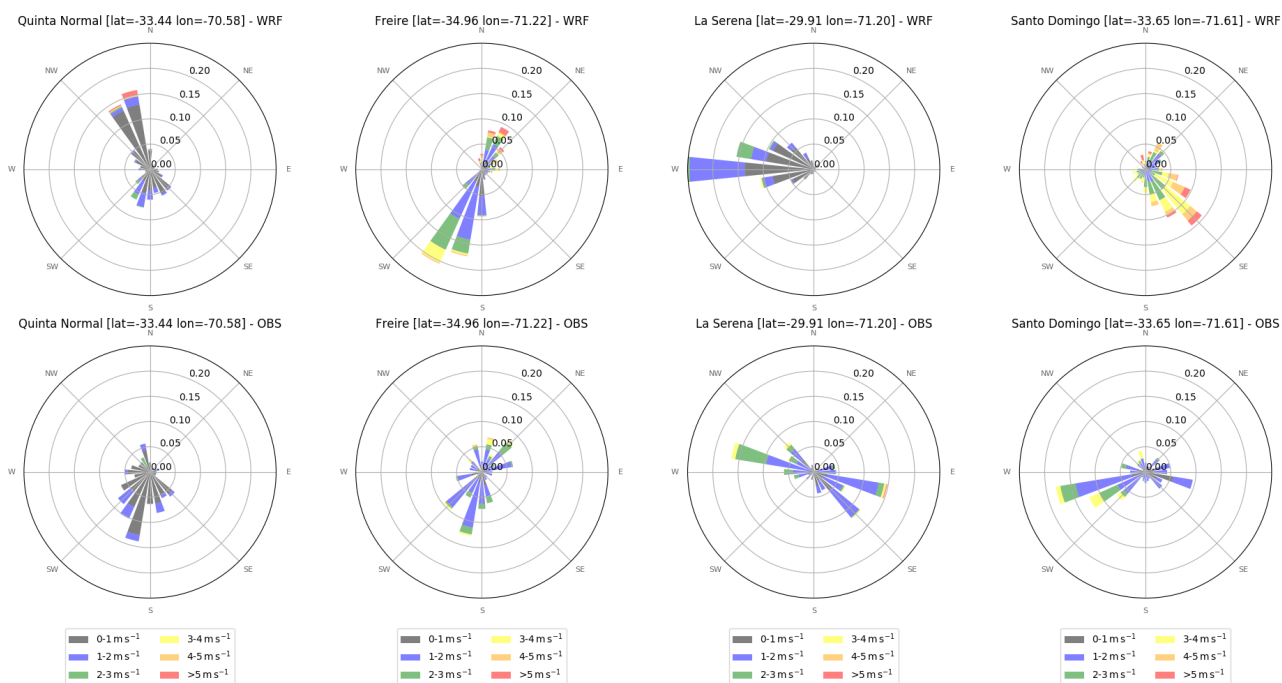
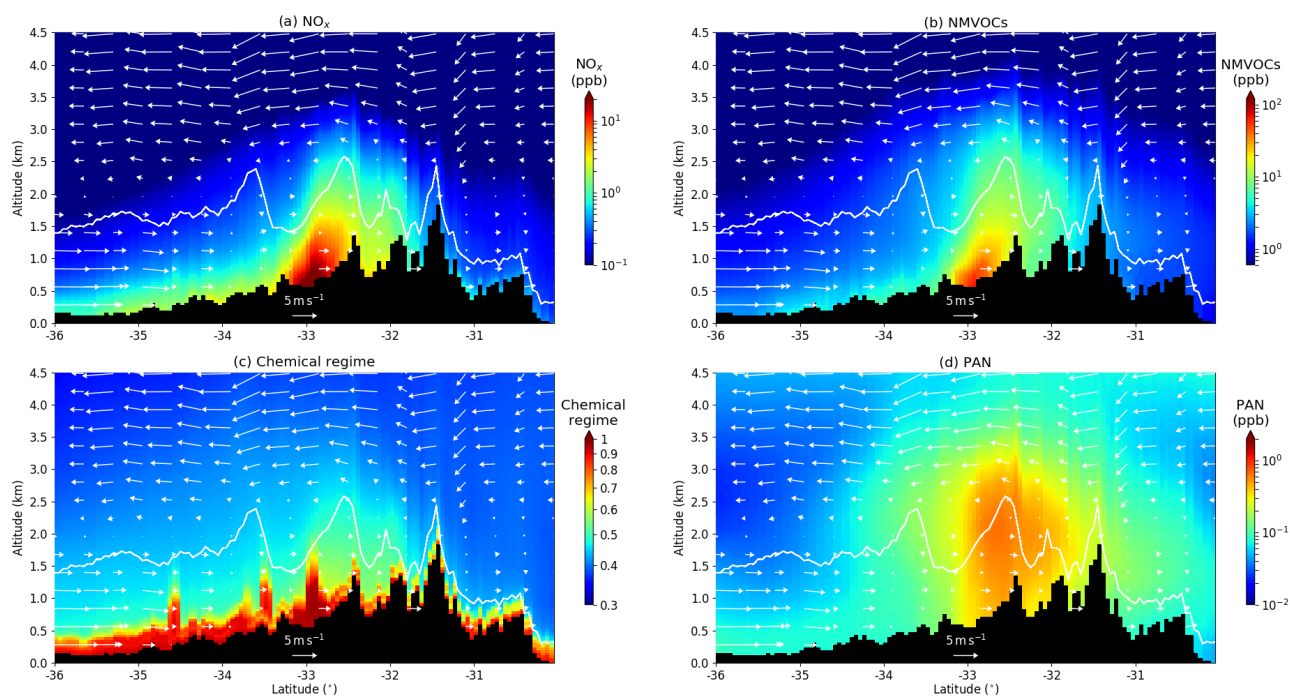


Figure A2. Same as Figure A1 for wintertime 2015.



**Figure A3.** (a) Simulated NO<sub>x</sub> concentrations (colormap), wind (arrows), afternoon boundary layer (white solid line) and terrain elevation (black area), along the summertime transect considered in Figure 9a. Average for summertime 2015. (b) same as (a) for NMVOC, (c) same as (a) for chemical regime, (d) same as (a) for Peroxyacetyl nitrate (PAN).